DOE/NASA/0167-7
NASA CR-174694
GARRETT NO. 31-3725(7)

ADVANCED GAS TURBINE (AGT) TECHNOLOGY DEVELOPMENT

SEVENTH SEMIANNUAL PROGRESS REPORT (JANUARY 1983 — JUNE 1983)

Engineering Staff of
Garrett Turbine Engine Company
A Division of The Garrett Corporation

DECEMBER 1983

Prepared for

NATIONAL AERONAUTICS AND SPACE ADMINISTRATION
Lewis Research Center
Cleveland, Ohio 44135
Under contract DEN3-167

for
U.S. DEPARTMENT OF ENERGY
Office of Vehicle and Engine Research and Development
Technology Development and Analysis Division
Washington D.C. 20585

DOE/NASA/0167-7
NASA CR-174694
GARRETT NO. 31-3725(7)

ADVANCED GAS TURBINE (AGT) TECHNOLOGY DEVELOPMENT

SEVENTH SEMIANNUAL PROGRESS REPORT
(JANUARY 1983 — JUNE 1983)

Engineering Staff of
Garrett Turbine Engine Company
A Division of The Garrett Corporation

DECEMBER 1983

Prepared for

NATIONAL AERONAUTICS AND SPACE ADMINISTRATION
Lewis Research Center
Cleveland, Ohio 44135
Under contract DEN3-167

for
U.S. DEPARTMENT OF ENERGY
Office of Vehicle and Engine Research and Development
Technology Development and Analysis Division
Washington D.C. 20585

TABLE OF CONTENTS

TABLE OF CONTENTS (Contd)

TABLE OF CONTENTS (Contd)

LIST OF FIGURES

LIST OF FIGURES (Contd)

LIST OF TABLES

1.0 SUMMARY

This report describes progress and work performed by the Garrett/Ford Team during January through June 1983 to develop technology for an Advanced Gas Turbine (AGT) engine for automotive applications. This work was performed for the Department of Energy under NASA Contract DEN3-167. This is the seventh in a series of semi-annual reports. Work performed during the first six periods (References 1 through 6) initiated design and analysis, ceramic development component testing, and test bed evaluation.

Project effort conducted under this contract is part of the DOE* Gas Turbine Highway Vehicle System Program. This program is oriented at providing the United States automotive industry the high-risk long-range technology necessary to produce gas turbine engines for automobiles with reduced fuel consumption and reduced environmental impact. Technology resulting from this program is intended to reach the marketplace by the early 1990's.

The advanced automotive gas turbine, when installed in a Ford vehicle (3000 pounds inertia weight), will provide:

- A combined federal driving cycle (CFDC) fuel economy of 42.8 miles per gallon based on Environmental Protection Agency (EPA) test procedures and Diesel No. 2 fuel. The AGT-powered vehicle will substantially give the same overall vehicle driveability and performance as a comparable production vehicle powered by a conventional spark-ignition powertrain system
- Emissions less than federal standards
- Ability to use a variety of fuels

The major accomplishments for this period are summarized in the following paragraphs.

*A list of abbreviations and acronyms is presented in Appendix D, herein.

1.1 Power Section Development

Extensive performance data were logged at speeds ranging from 50,000 to 85,000 rpm for a range of variable unit guide vane (VIGV) settings on S/N 003, Build 8. Review of test data and comparison with computer performance models indicated a high interpath leakage; Fuller's earth was injected to locate the leak. Indications showed a leakage at the turbine shroud/transition duct/flow separator housing. A new seal ring was designed for this area with data indicating a 35 percent power increase. Other leakage areas were noted in subsequent builds and efforts to correct these problems are underway.

During January to April 1983, forced rotor vibration emanating from the gearbox precluded full load testing at speeds above 85,000 rpm. A quill shaft gearbox was introduced and the forced vibration problem was resolved. However, self-excited subsynchronous motion has been encountered, which currently is hindering full speed operation.

Performance is an important factor in evaluating the potential of the advanced automotive gas turbine. The Garrett/Ford AGT101 has a sea level, 59°F, CFDC fuel economy target of 42.8 mpg, with diesel DF-2, in a 3000-pound automobile. This target, established for the Reference Powertrain Design (RPD) at the beginning of the project, recently has been reviewed to determine the position of the AGT101 component/engine development activities, relative to goals, so that project resources could be properly allocated. This evaluation shows that when using tested component efficiencies the calculated CFDC mileage in the baseline vehicle and drive line (Ford 1980 data) is 43.3 mpg.

To date 153.3 hours of testing have been accumulated on the three test bed engines.

1.2 Compressor

Redesign activities have been initiated on

the impeller to address fabrication of near net shape powder metal (PM) die forgings while retaining or improving the demonstrated performance.

1.3 Turbine

The baseline AGT101 turbine rotor has been redesigned to increase thickness with a modified blade shape to improve ceramic manufacturing capabilities.

1.4 Combustor

Facility problems delayed testing of the reworked simplex Delavan nozzle. Heat transfer analysis identified potential heat paths that could over heat the nozzle and cause fuel coking near the fuel distribution ring. Redesign of this area has alleviated the problem and hardware is in fabrication.

1.5 Regenerator

NGK is developing extruded rectangular cell matrixes having cell densities of 1100 and 1380 cells/in^2 with 0.0047 and 0.0042 inch wall thicknesses. Phase 4 seals, which include a cooled hot side crossarm seal for 2000°F operation, are being developed by Ford.

Hot regenerator rig test data were recorded for two different seal build clearances and a range of airflows up to 30 lb/min. Data indicates seal leakage of 8 percent at idle conditions.

1.6 Ceramics

Testing, analysis, and fabrication data has been compiled and have provided sufficient information to perform the first overall design improvement for components that have proven to be difficult to fabricate or are highly stressed; ie, inner diffuser housing, outer diffuser housing and turbine shroud.

Build 6 of the ceramic structures rig was completed and the unit installed in the test facility. Approximately 16 hours of testing was conducted with several acoustic signals above 85 db. Following initial testing the unit was partially disassembled. Disassembly revealed that a failure had occurred. Results of fractography and inspection showed a mechanical interference to be the cause of failure.

Two turbine rotors were thermally cycled in the hot turbine rig. The second rotor tested now is qualified for full speed/load operation at 1600°F and is available for engine testing.

1.7 Rotor Dynamics

Numerous tests on the rotor dynamics and single bearing test rigs were accomplished. Variations of foil bearing sway space, stiffness, damping capacity, power dissipation and stability were evaluated. Additional work continues to resolve the self-excited subsynchronous motion now limiting engine full speed operation.

2.0 INTRODUCTION

This report is the eighth in a series of Semi-annual Technical Summary Reports for the Advanced Gas Turbine (AGT) Technology Development Project, authorized under NASA Contract DEN3-167 and sponsored by the Department of Energy (DOE). This report has been prepared by The Garrett Turbine Engine Company (hereinafter referred to as Garrett), a Division of The Garrett Corporation, and includes information provided by Ford Motor Company, The Carborundum Company, and AiResearch Casting Company. The project is administered by Mr. Roger Palmer, Project Manager, NASA-Lewis Research Center, Cleveland, Ohio. This report presents plans and progress from January through June 1983.

Project effort conducted under this contract is part of the DOE Gas Turbine Highway Vehicle System Program. This program is oriented at providing the United States automotive industry the high risk, long range technology necessary to produce gas turbine engines for automobiles that will have reduced fuel consumption and reduced environmental impact. The intent is that technology resulting from this program be capable of reaching the marketplace by the early 1990's.

The advanced AGT, when installed in a Ford vehicle (3000 pounds inertia weight) would provide:

- A CFDC fuel economy of 42.8 miles per gallon based on EPA test procedures and DF-2. The AGT-powered vehicle shall give substantially the same overall vehicle driveability and performance as a comparable production vehicle powered by a conventional spark-ignition powertrain system
- Emission less than federal standards
- Ability to use variety of fuels

The Garrett/Ford advanced AGT has been designated the AGT101.

The program is oriented toward developing the AGT101 gas turbine long range high risk technology such that the automotive industry can carry that technology forward to production in the 1990's. Emphasis on ceramics, gas bearings, low emission combustion and improved component performance continue. The AGT101 gas turbine is being used as a test bed in which to develop these technologies.

The program schedule is depicted in Figure 1. The program continues technology work through FY85 and culminating in demonstration of the original goals of engine specific fuel consumption, power output, and emissions. In addition, the viability of ceramics will have been demonstrated in the AGT101 test beds, and the potential of economically producing the ceramic parts in automotive production quantities will have been assessed. When these goals are achieved, Ford will be in a position to proceed, without Government support, through the typical preproduction tasks which then could lead to production in the 1990's.

The primary technology challenges in the program continue to be ceramic component and related high performance gas turbine aerothermodynamic component development for the AGT101. The AGT101 nominally is a 100 shp engine, capable of speeds to 100,000 rpm and operating at turbine inlet temperatures (TIT) to 2500°F with a specific fuel consumption level of 0.3 over much of the operating range.

This report reviews the power section (engine) effort conducted to date, followed by a review of the component/ceramic technology development. Appendices include reports of progress from Ford, AiResearch Casting Company, and the Carborundum Company.

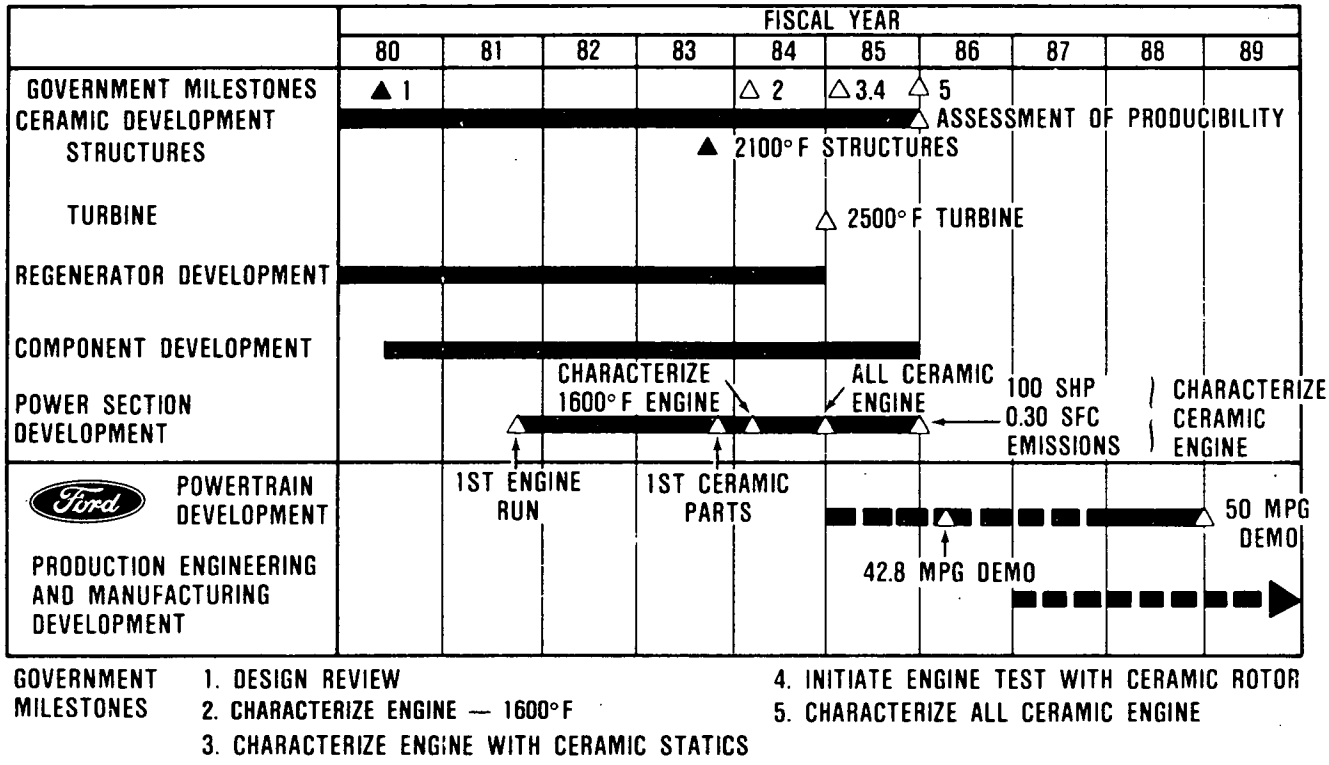

Figure 1. AGT101 Program Schedule.

3.0 POWER SECTION DEVELOPMENT

Testing continued through the reporting period on AGT101 engines S/Ns 001 and 003. S/N 002 engine was converted to accept ceramic structures during the same period. System performance, analytical modeling and rotor dynamic development constituted the primary areas of power section development.

3.1 Engine Performance Development

Engine S/N 003 Build 8 testing was initiated in January 1983. Performance data were logged at speeds ranging from 50,000 to 85,000 rpm for a range of VIGV settings. Performance testing included acquisition of key pressures, pressure drops and inlet flow as shown in Figure 2. Testing above 85,000 rpm was hindered by rotor dynamic instability.

Review of the test data and comparison with computer performance predictions pointed to high interpath leakage as the major cause of low output power. Therefore, Fuller's Earth was injected into the engine to aid in locating leak points.

The engine was disassembled and inspected. The primary leakage path shown in Figure 3 was through the transition duct/turbine shroud/flow separator housing seal rings. Figure 4 shows Fuller's Earth leakage traces between the flow separator housing and the transition duct and in the flow toward the LP exhaust section. This same leakage is depicted in Figure 5 as it passes by the turbine shroud and out the LP exhaust. Figure 6 shows another leakage path by the exhaust housing sealing rings around the flow separator housing, and Figure 7 reveals the leakage around the regenerator seals (primarily at the corners of the diaphragms).

As a result of S/N 003 Build 8 test and teardown, a new sealing ring design was implemented in the turbine shroud area (Figure 8). The intent of this seal modification was to minimize the effect of thermal out-of-round conditions of the sealing surface on the flow separator housing. The engine was retested (Build 9) and the TIT decreased from 1380°F at no load idle to approximately 1250°F. This indicates a reduction in overall leakage. SHP increased over the previous build from 6.55 to 8.82 at 70,000 rpm; a 35-percent power increase. Table 1 shows comparative performance data at 70,000 rpm for the original and modified seal configurations.

Analysis of the Build 9 performance data using the AGT101 computer model indicated that excessive leakage existed into the regenerator bore cavity. This cavity receives the leakage flows from both regenerator inner diameter seals plus the exhaust housing piston rings. Test provisions were made to quantify total bore leakage on S/N 003, Build 10. The bore cavity was fitted with a manifold and aspirated through a measuring section. The bore leakages measured at 50,000 rpm are shown in Figure 9. Accurate measurements at higher speeds were not possible due to manifold choke conditions.

3.2 Engine Performance Match Model

Concurrent with the engine performance characterization testing, the engine performance match model was reviewed, updated and checked out. This computer engine analysis model combines the test aerodynamic maps and regenerator off-design analysis with a comprehensive leakage and internal heat transfer model. Figure 10 schematically shows the leakage and heat transfer paths considered. Four heat transfer and eight leak paths are included.

Table 2 tabulates match model percent leakages derived for a test point taken February 25, 1983. Computed leakage for this test point is 13.75 percent of inlet flow compared with the 1600°F engine goal of 9.5 percent (7 percent regenerator, 2 percent foil bearing, 0.5 percent overboard).

3.3 Engine Rotor Dynamic Development

During engine tests, January through April 1983, forced rotor vibration emanating from the gearbox precluded full load testing at

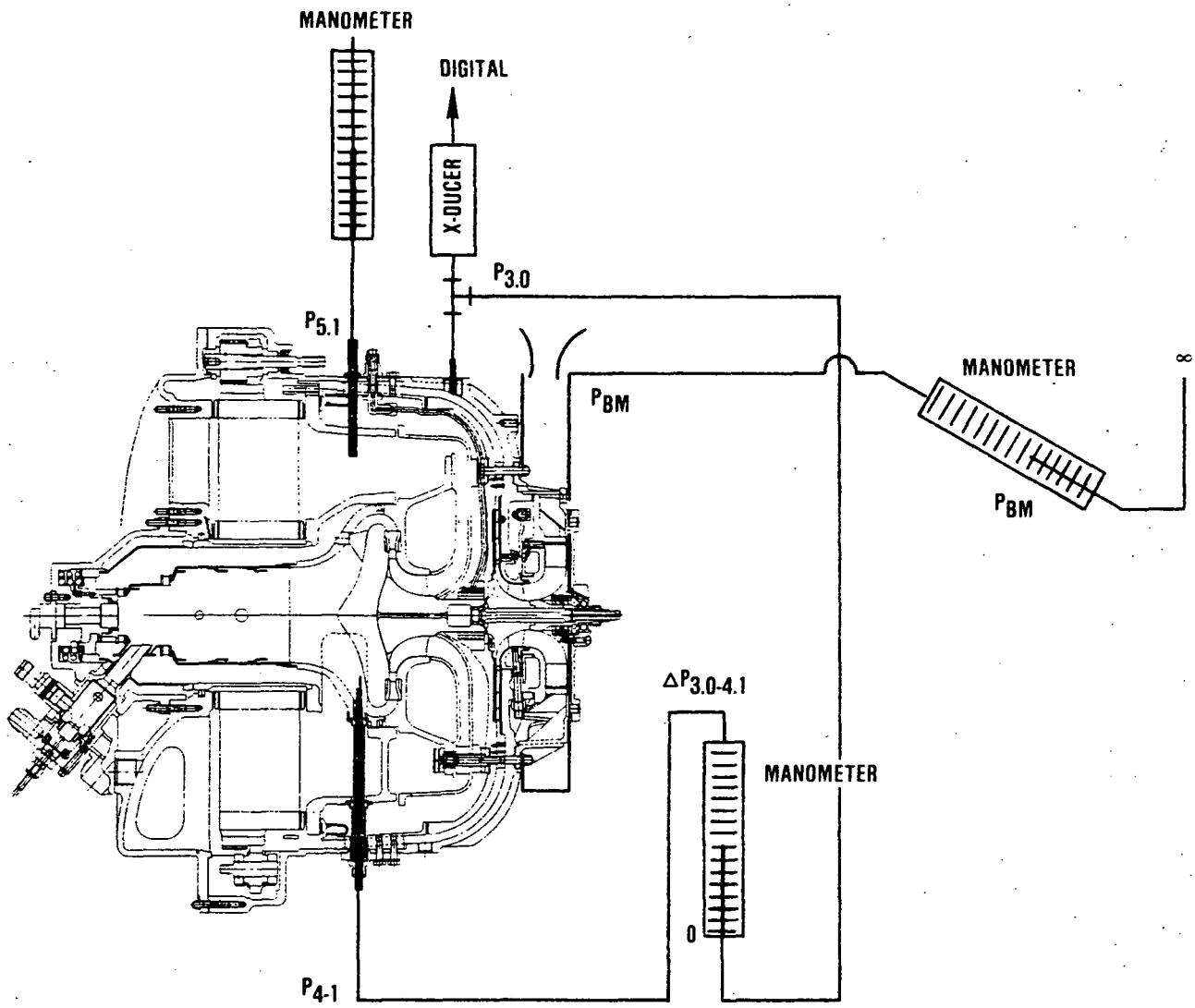

Figure 2. Pressure Instrumentation Schematic.

speeds above 85,000 rpm. This problem was encountered with all engine builds using the direct coupled gearbox configuration.

The forced response of the rotor (at 1 and 2 times gearbox output speed) is excited through the planet/sun mesh. Typical dynamic response is shown in Figures 11 through 13. Note that the response is both load and speed dependent.

To combat the forced vibration sources in the gearbox, the quillshaft gearbox configuration was introduced into the test program in May 1983.

The quillshaft gearbox, intended to decouple gearbox and rotor vibrations, was first tested on engine S/N 003 Build 11. By the time S/N 003 Build 12 was tested, sufficient testing had been accomplished to verify that the forced vibration problem from gearbox sources had been eliminated.

Later in the testing of Build 12, self-excited subsynchronous motion at a magnitude

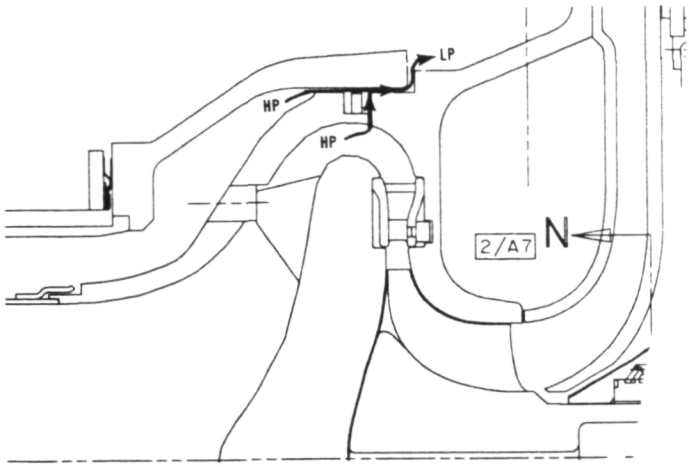

Figure 3. Primary Leakage Path.

Figure 4. Fuller's Earth Traces - Flow Separator Housing/Transition Duct.

of 4 mils halted an acceleration at 78,300 rpm. The frequency of vibration was 86 Hz. Numerous engine tests in May and June 1983 resulted in similar encounters with self-excited instability in the first rigid body mode.

The rotor and support system was reviewed in an attempt to identify possible causes of instability. In June 1983, during instrumentation refurbishment, the carrier was had a loose

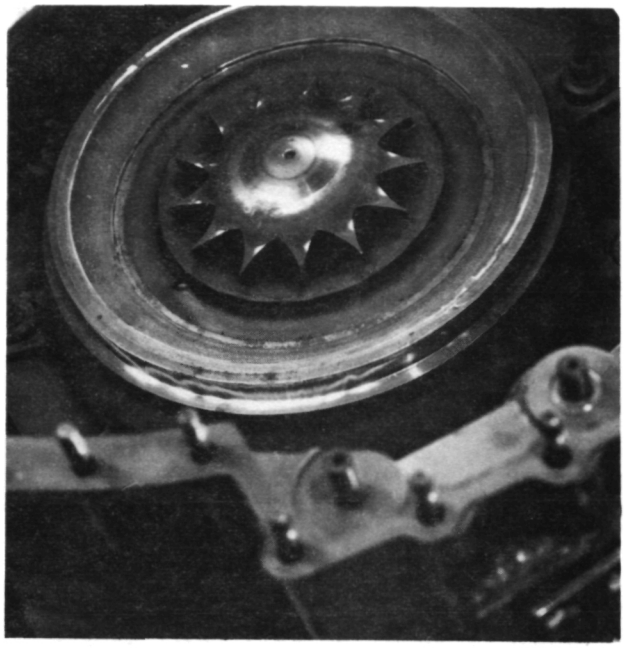

Figure 5. Fuller's Earth Traces - Turbine Shroud.

Figure 6. Fuller's Earth Traces - Regenerator Shield Piston Ring.

(1-2 mils) fit in the mating housing with both parts at approximately 400°F. Closer scrutiny revealed the thermal expansion coefficients to be dissimilar enough to cause the loose fit. New housings are being made from 17-4PH

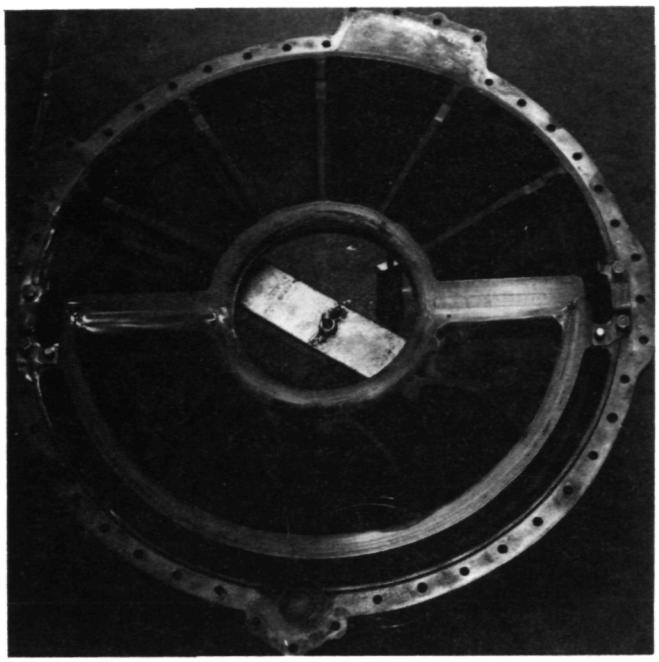

Figure 7. Fuller's Earth Traces - Regenerator Seals.

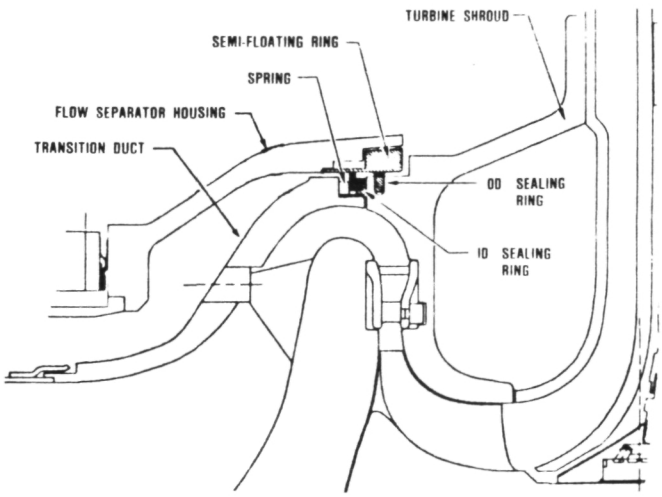

Figure 8. Sealing Ring Redesign.

replacing the present CRES 347 housing. This should preclude the possibility of carrier fits loosening since the expansion coefficients of the new housing and foil carrier (made of 4340) essentially are the same.

In an effort to solve the rotor stability problem, a parallel effort is underway to increase foil bearing stiffness, introduce shaft damping for the first mode, and to minimize cross-coupling forces within the bearing. Alternate foil bearing configurations are in development including changes in foil count, foil thickness, and sway space.

3.4 Performance Evaluation

To determine the position of the AGT101 component/engine development activities, relative to goals, and so that project resources could be properly allocated, an evaluation using tested component efficiencies, was performed. The calculated CFDC mileage in the baseline vehicle and drive line (Ford 1980 data) was 43.3 mpg. The following sections describes the analysis.

3.4.1 Compressor and Turbine Efficiency

The actual compressor and turbine test maps were substituted for those of the RPD. Both maps were simultaneously used, instead of one at a time, because of the importance of component matching. The best match (and thus CFDC mileage) was obtained by scaling up the tested turbine 11.3 percent in flow capacity (11.3 percent wider stator passage). This match has no risk and no negative impact on efficiency. This means that the aerodynamic performance now available is sufficient. Therefore, no new technology improvements are needed and only minor changes are contemplated.

Overall, the AGT101 aerodynamics now meet RPD goals. Future work in these areas is aimed at minor improvements in producibility without losing present efficiency levels.

3.4.2 Regenerator

NGK has extruded core segments that exceed RPD goals of hydraulic radius and wall thickness in an MAS core with equilateral triangle matrix (Table 3). Ford has tested many samples of matrices in the past and has a data base that was used to set RPD goals.

TABLE 1. ENGINE S/N 003 TEST COMPARISON

			1-24-83 Engine Test (Before Fix) Build 8	2-25-83 Engine Test (After Fix) Build 9
VIGV Position	IGV	deg	0	0
Rotor Speed	N	rpm	70,060	70,440
Bellmouth Weight Flow	$W_{1.0}$	lb/sec	0.4100	--
Compressor Corrected Flow	$(W \quad / \quad)_c$	lb/sec	0.4291	--
Compressor Pressure Ratio	PR_C	--	2.421	2.426
Turbine Pressure Ratio	PR_T	--	2.218	--
Ambient Pressure	$P_{1.0}$	psia	14.246	14.063
Compressor Discharge Pressure	$P_{3.0}$	psia	33.92	34.12
HP Flow Path P	P_{HP}	in-H_2O	37.70	--
Turbine Inlet Pressure	$P_{4.0}$	psia	32.56	--
Low Pressure Flow Path P	P_{LP}	in-H_2O	12.10	--
Ambient Temperature	$T_{1.0}$	^oF	57	72
Compressor Discharge Temperature	$T_{3.0}$	^oF	263	285
Regenerator HP Inlet Temperature	$T_{3.1}$	^oF	298	316
Regenerator HP Discharge Temperature	$T_{3.5}$	^oF	1061	1117[3]
Turbine Inlet Temperature	$T_{4.0}$	^oF	1581	1585
Regenerator LP Inlet Temperature	$T_{5.1}$	^oF	--	1245
Engine Exhaust Temperature	$T_{5.5}$	^oF	407	410
Regenerator Temperature Effectiveness	E_r	%	--	0.862[3]
Fuel Flow (LHV = 18,860 Btu/lb)	W_f	lb/hr	8.89	8.68
Aerodynamic Power	HP_A	hp	(9.64)	(11.91)
Bearing and Windage Loss	HP_B	hp	(1.13)	(1.13)
Gearbox Loss	HP_G	hp	(1.96)	(1.96)
Net Dyno Power	HP_N	hp	6.55	8.82

NOTES:

1. Corning Core, both cases
2. January 24, 1983 test had 1.5 percent bellmouth ΔP, analysis says P, ΔP_{INLET}, $T\sigma$ should yield same power in both tests (even trade-off)
3. Based on only one thermocouple at Station 3.5
4. Data in parenthesis is calculated

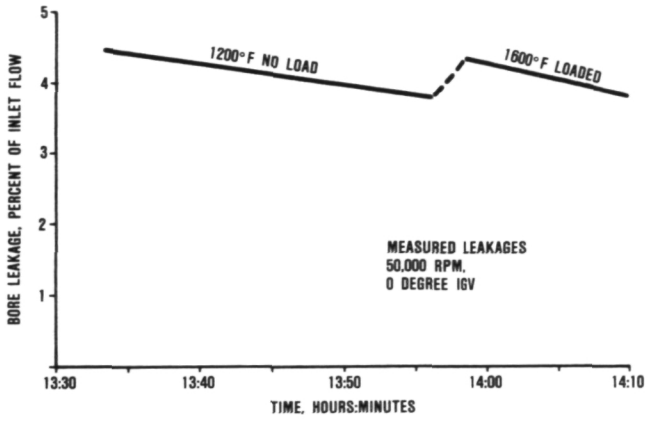

Figure 9. S/N 003 Regenerator Bore Leakage.

This new core data was used in the engine performance analysis in conjunction with the tested aerodynamic maps and produced 43.3 mpg. All other elements of the RPD regenerator are unchanged including the regenerator seal leakage of 3.6 percent, and the 2000°F RPD operating limit for regenerator inlet temperature level; 2000°F was set as the goal for the RPD maximum operating limit. Over 1700 hours of testing has been accomplished at Ford at temperatures to 2000°F. Thus the 2000°F goal is achievable.

3.4.3 Heat Loss, Leakage Flows, and Pressure Losses

All these values are unchanged from those used in the RPD and still appear achievable in 1985.

This analysis projects an outstanding engine SFC map as shown in Figure 14.

Vehicle performance Figure 15 presents CFDC mileage and 2-second distance traveled versus idle speed; 48,300 rpm idle speed will satisfy the 2-second distance (8 feet) and yield 43.3 mpg which is 0.5 mpg above the original RPD goals. Figure 16 shows that steady-state fuel economy peaks at 76 mpg at 34 mph.

3.5 Summary

Table 4 and Figure 17 depict the current test history of the AGT101 (1600°F) engine. As discussed, performance testing indicates excessive internal leakage in the regenerator bore and turbine shroud piston ring areas. Efforts are underway to resolve these problems using a better piston ring mounting arrangement and alternate sealing mechanisms.

Driven excitation of the rotating group appears to be resolved with the incorporation of the quillshaft gearbox. However, self-excited subsynchronous motion is now emerging as a speed limiter. Review of the builds, bearings, balance, and testing data are currently underway to resolve this problem.

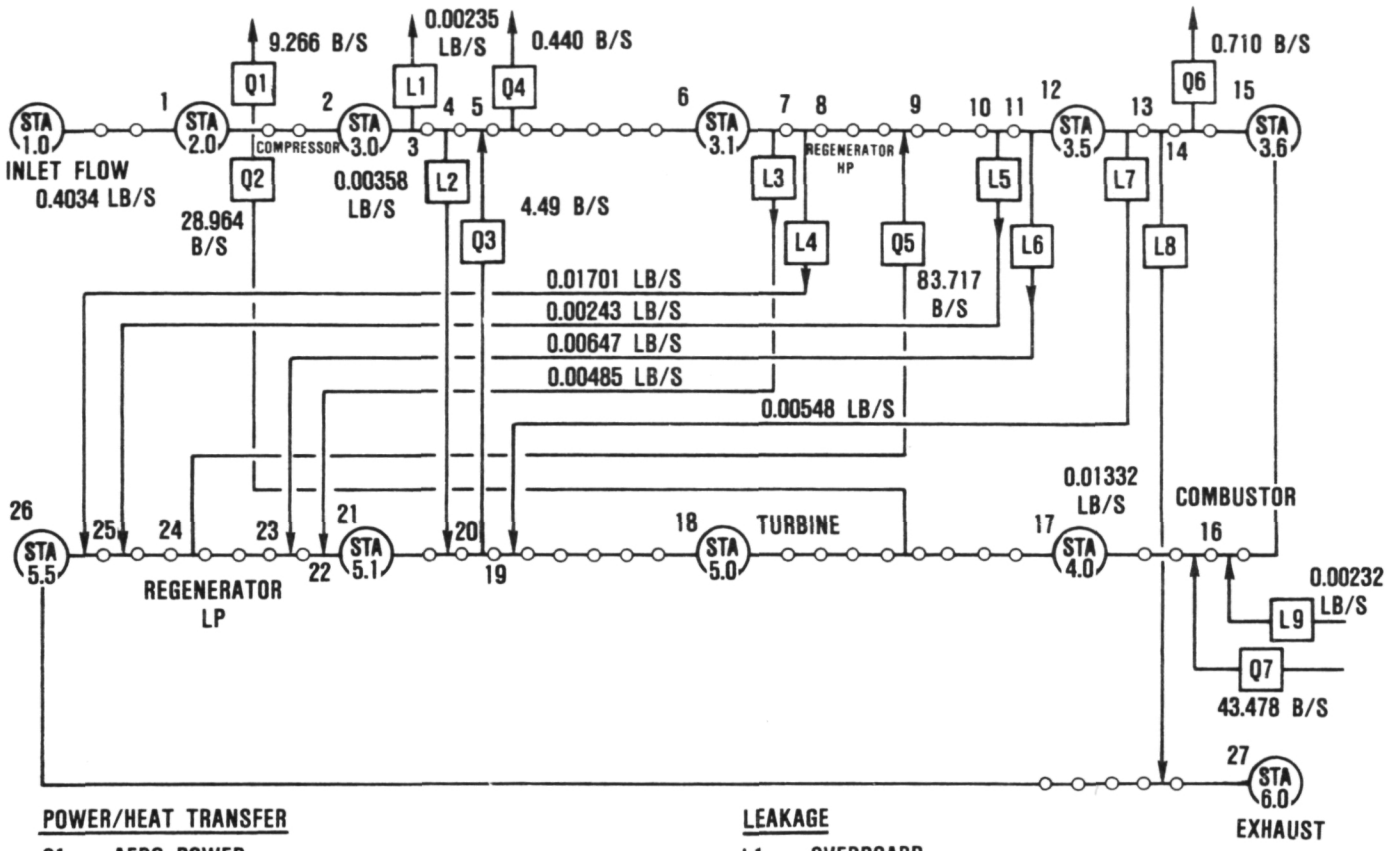

POWER/HEAT TRANSFER

Q1 — AERO POWER
Q2 — TURBINE POWER
Q3 — TURBINE DISCHARGE — COMPRESSOR DISCHARGE TRANSFER
Q4 — COMPRESSOR DISCHARGE — AMBIENT TRANSFER
Q5 — REGENERATOR HEAT TRANSFER
Q6 — COMBUSTOR DOME-AMBIENT TRANSFER
Q7 — FUEL FLOW * [LHV + (0.5 * T_{AMB})] * η_{COMB}

LEAKAGE

L1 — OVERBOARD
L2 — FOIL BEARING
L3 — REGENERATOR 3.1-5.1
L4 — REGENERATOR 3.1-5.5
L5 — REGENERATOR 3.5-5.5
L6 — REGENERATOR 3.5-5.1
L7 — TURBINE PISTON RINGS
L8 — EXHAUST PISTON RINGS
L9 — FUEL FLOW (TREATED AS NEGATIVE LEAKAGE FROM MASS BALANCE VIEWPOINT)

Figure 10. Mass and Energy Balance Schematic, S/N 003, Build 9, 70,000 RPM.

TABLE 2. PERFORMANCE ANALYSIS LEAKAGE.

Leakage Area	Percent of Inlet Flow	AGT101 (1600°F) Goal
Overboard Leakage	0.58	0.5
Foil Bearing Flow	0.89	1.0
Regenerator Seal (HP Inlet-LP Inlet)	1.20	
Regenerator Seal (HP Inlet-LP Discharge)	4.22	5.0
Regenerator Seal (HP Discharge-LP Discharge	0.60	
Regenerator Seal (HP Discharge-LP Inlet)	1.60	
Shroud Piston Rings	1.36	1.5
Exhaust Housing Piston Rings	3.30	1.0
Total Percent of Inlet Flow	13.75	9.0

TEST: 2-25-83; 70,000 RPM; 72°F; 14.06 PSIA

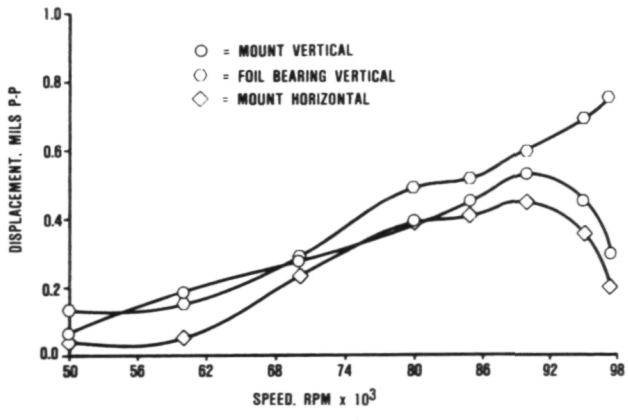

Figure 11. Synchronous Response on Acceleration With No Load.

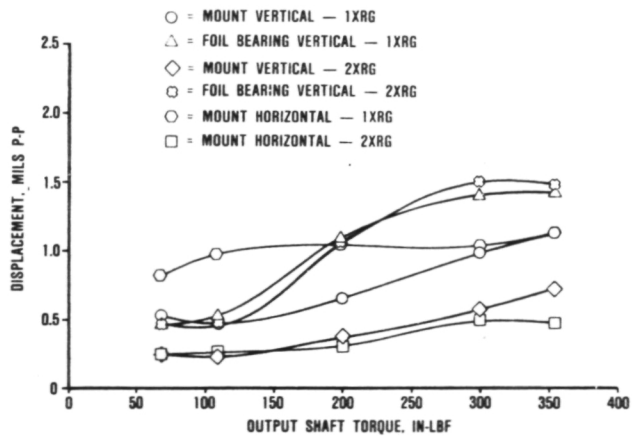

Figure 12. Forced Response at 80,000 RPM Versus Torque.

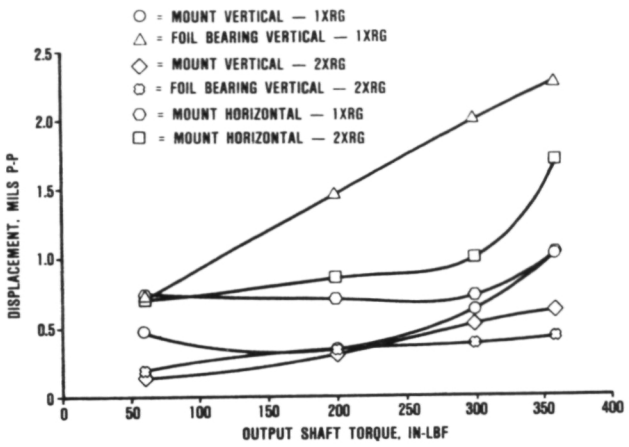

Figure 13. Forced Response at 85,000 RPM Versus Torque Applied at Loader.

TABLE 3. 1982 NGK CORE DATA.

Hydraulic diameter	=	0.0194 inch
Surface density	=	1816 ft^2/ft^3
Flow area ratio	=	0.734
Web thickness	=	0.0030 inch
(j) (Re)	=	3.93

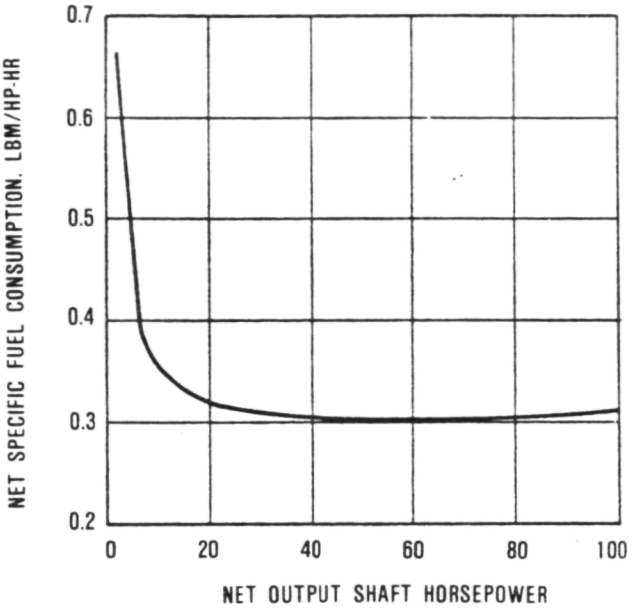

Figure 14. AGT101 Specific Fuel Consumption Versus Horsepower.

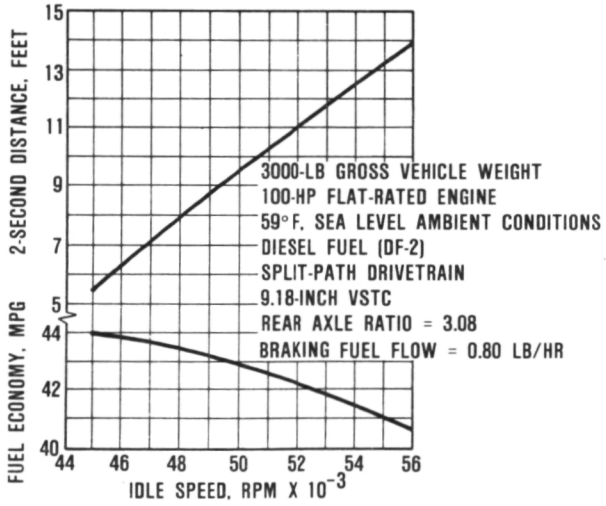

Figure 15. Idle Speed Affects Fuel Economy and Performance.

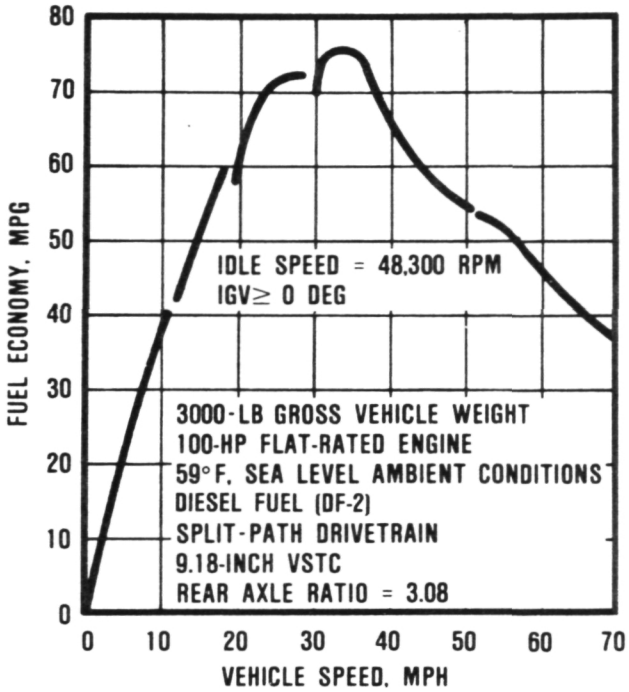

Figure 16. AGT101 (2500°F) Steady-State Mileage.

TABLE 4. ENGINE TESTING THROUGH JUNE 1983

Power Section S/N	Builds	Starts	Operating Time hours
001	11	121	77.0
002	4	70	20.7
003	15	138	55.6
	30	329	153.3

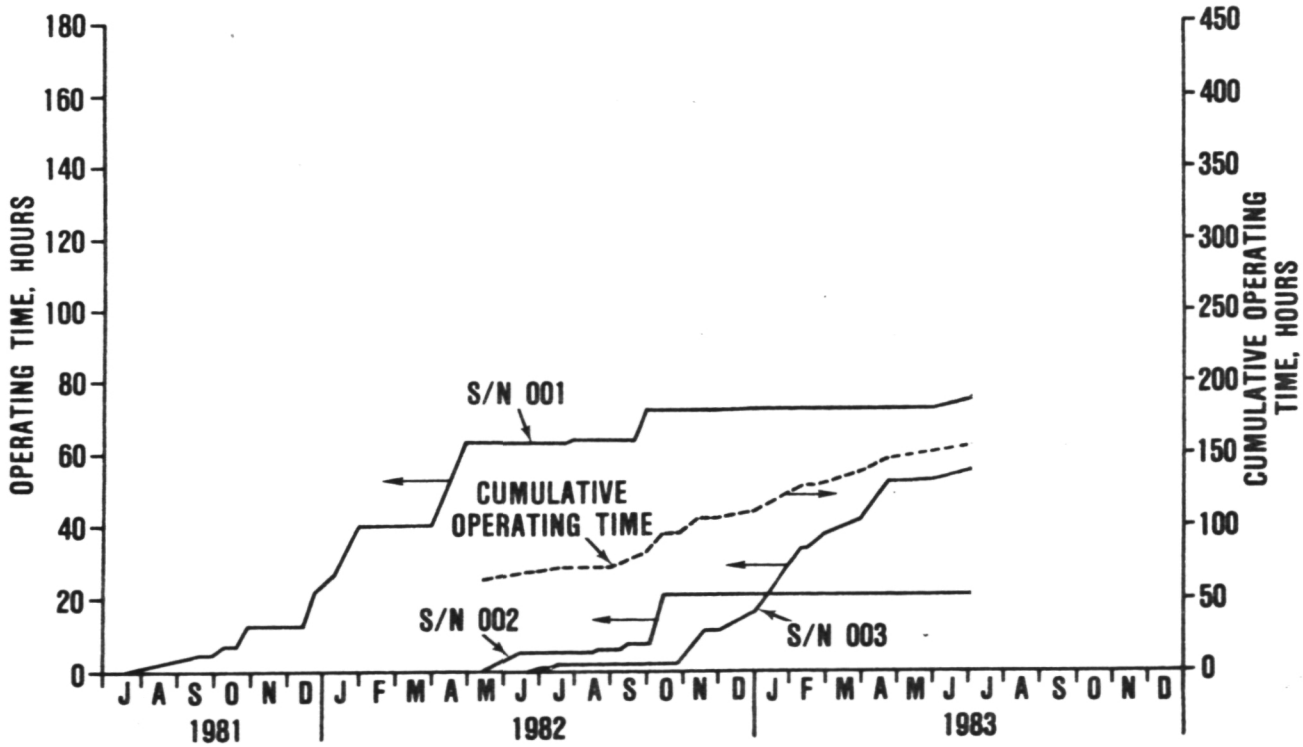

Figure 17. AGT101 Power Section Test Time.

4.0 COMPONENT/SUBSYSTEM DEVELOPMENT

Component/subsystem development activities during this reporting period were concentrated on supporting AGT101 1600°F engine testing, ceramic development, combustion nozzle tests, and hot regenerator testing. Figure 18 shows the performance rating stations for the AGT101 engine and components.

The following sections discuss major efforts and accomplishments during the reporting period for each component/subsystem.

4.1 Compressor

Redesign activities have been initiated on the impeller to address fabrication of near-net-shape powder metal (PM) die forgings while retaining or improving the currently demonstrated performance characteristics (Reference 6). To accomplish this, based on past Garrett experience, the impeller will be redesigned using the straight line element (SLE) blade shape definition. This technique has been refined to allow SLE approximation of arbitrary blade shapes by fitting each blade surface separately. The basis for the new design is to keep the best features of the current design while improving those areas indicated by the test results.

4.2 Turbine

To improve ceramic manufacturing cap-

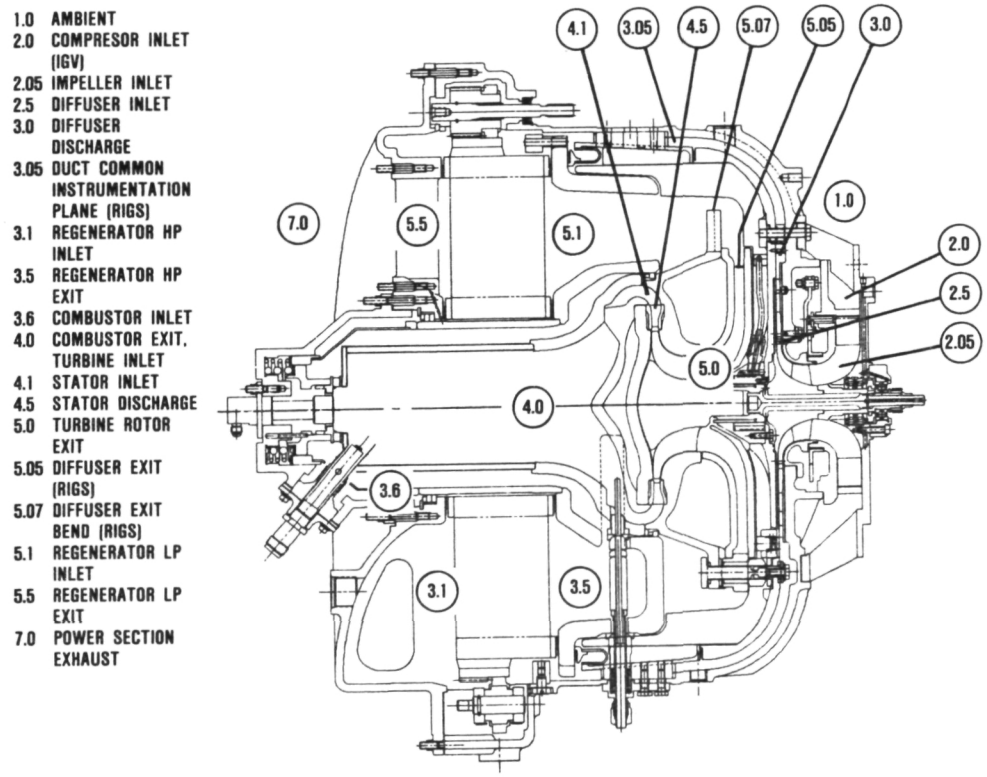

Figure 18. Performance Rating Stations.

abilities, the baseline rotor has been redesigned with increased blade thickness and modified blade shapes. The complete redesign is described in the following sections:

4.2.1 Radial Rotor Design Philosophy

The rotor aerodynamic design is the determination of the blade geometry at hub, mean, and shroud (and other streamline locations as required), which satisfies the optimum velocity diagram and distribution consistent with the work output requirement. The radial rotor is designed through a number of steps, which are given in the flow chart in Figure 19. Figure 20 is included to define section cuts through the rotor for tooling and inspection stations.

The baseline ceramic rotor used "Z-sections" in the shape of a "soda bottle." This is shown in Figure 21 by the solid line. From a manufacturing standpoint, modifying this shape to that shown by the dotted line in Figure 21 is desirable. In addition, rotor normal thickness at the inducer tip was modified from 0.030 to 0.040 inch to ease manufacturing. The comparison of the normal thickness distributions between the original and redesigned rotors are presented in Figure 22.

4.2.2 Rotor Blade Angle Distribution

The redesigned rotor preserved the original blade angle distribution to match the baseline velocity diagram.

The rotor blade angle distribution for the hub, mean, and shroud streamlines are shown in Figure 23.

4.2.3 Rotor Blade Loading

Blade surface velocity distributions, calculated from the axisymmetric flow solution at the shroud, mean, and hub streamlines are shown in Figures 24 through 26 and compare baseline design rotor loadings.

The figures illustrate the hub-to-shroud variations in the surface velocities and the blade loadings, as well as the variations along the flowpath. The blade is more heavily loaded along the shroud than elsewhere because of lower solidity. Loading near the rotor inlet where the flow is nearly radial, is considerably higher than the loading near the rotor exit where the flow is nearly axial. A comparison of blade loadings between the redesigned and baseline rotor, shows that the redesigned rotor loading at the exit converges to a single value (which was lacking in the baseline design). Theoretically, this means higher work extraction in the redesigned rotor. However, the redesigned rotor loading indicates some diffusion downstream of the throat when compared with baseline rotor design. The performance penalty due to the surface diffusion probably offsets any benefit that could be claimed due to loading closure. Thus, no efficiency changes in the redesigned rotor are expected.

4.3 Combustion

4.3.1 Reacting Element Tests

Combustion system development was restricted during this period by hardware and facilities problems.

Scheduled testing of the Simplex fuel nozzle, Figure 27, commenced using the fully opened radial inflow swirler at test conditions described in Reference 6. However no useful data was obtained from this run due to foreign material trapped in the fuel distribution ring which migrated to the injection orifices and resulted in plugging. SEM analysis of the plugging material indicated it to be parent nozzle material.

Both the fuel distributor ring and injection holes were free of any carbon deposit. This is significant, since at the operating condition, and duration, for which the nozzle was run, thermal degradation of the fuel can occur.

Calculation using the nozzle heat transfer data of Section 4.3.2 herein, indicates that for the conditions tested, some carbon formation

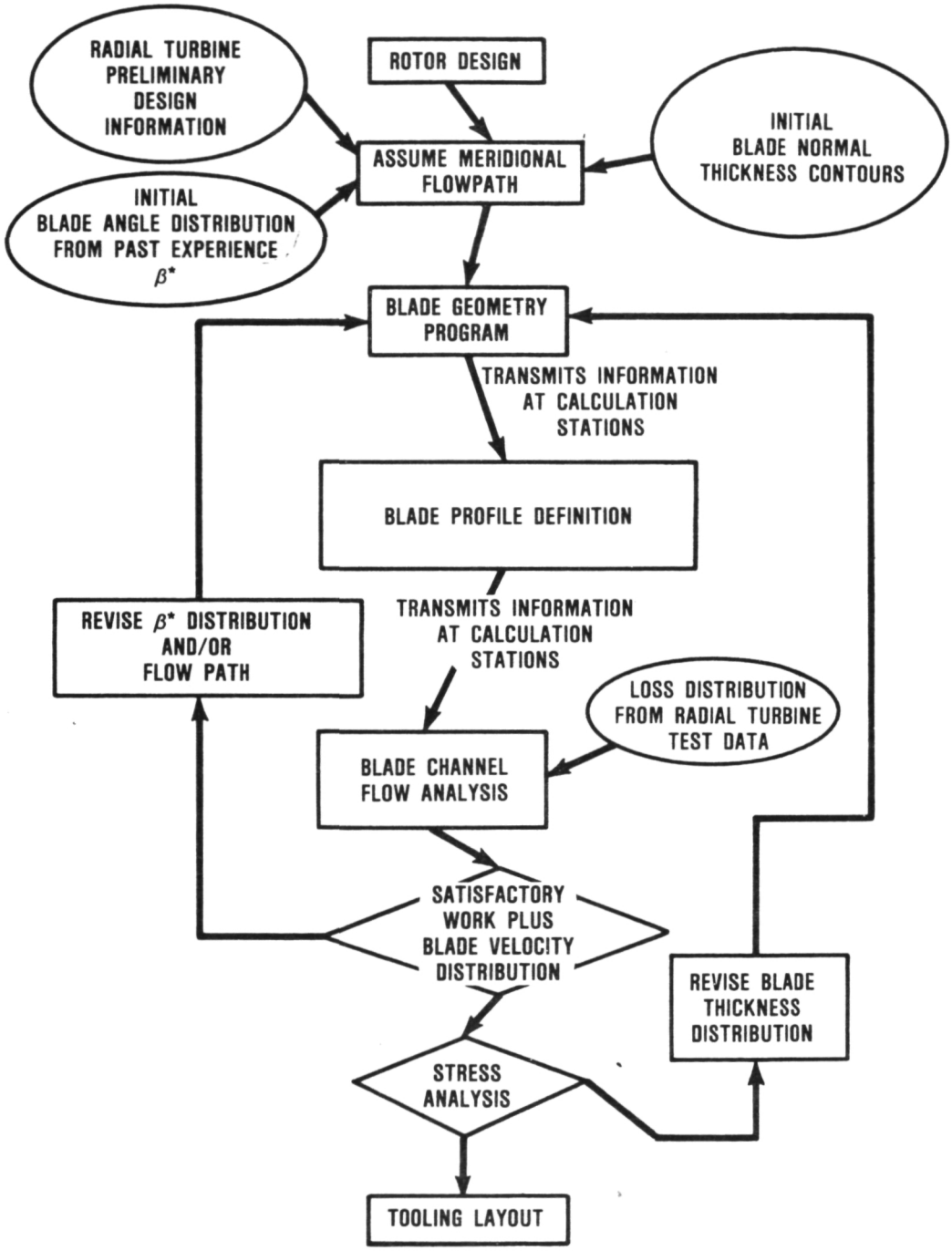

Figure 19. Radial Turbine Design Flow.

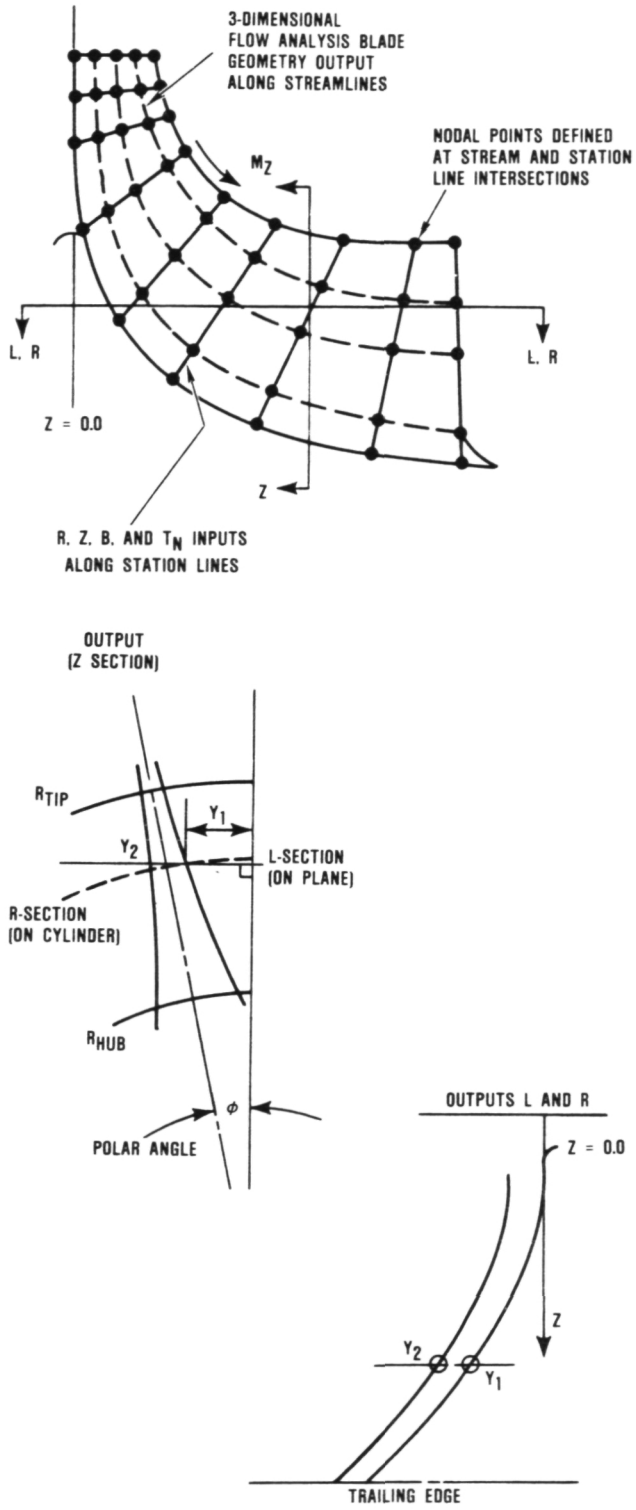

Figure 20. Radial Rotor Geometry Program.

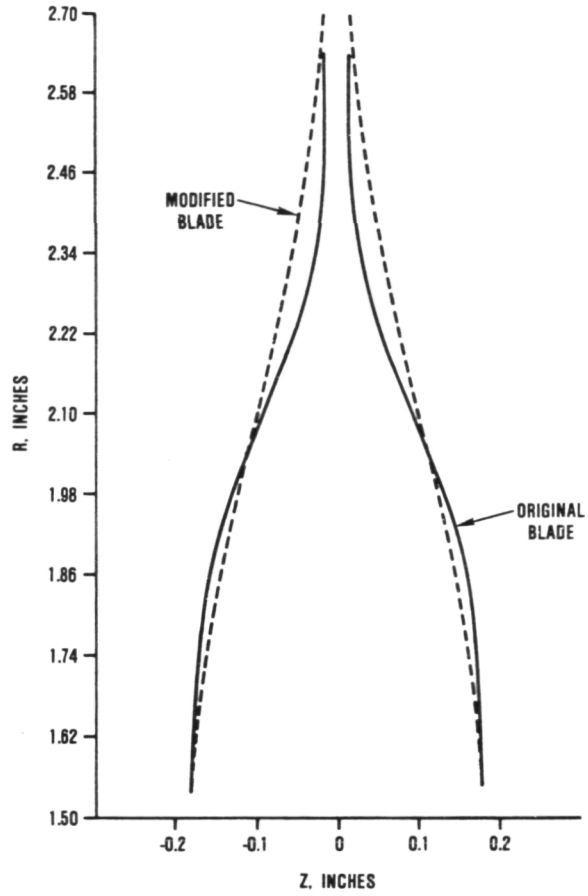

Figure 21. AGT101 Ceramic Rotor Z-Section.

should have occurred. The fact that deposition was not experienced is attributed to the action of the air assist.

The nozzle was reworked and rescheduled for development testing. Immediately prior to testing, facility problems were incurred on the second-stage process air preheater, which raises the temperature of air delivered to the test section from 1300 to 2000°F. The unit was removed from the test facility and investigations are underway.

4.3.2 Fuel Nozzle Heat Transfer Analysis

Fuel thermal degradation and deposition/coking of fuel passageways can be a severe problem at elevated combustor inlet temperatures. The combustor entry temper-

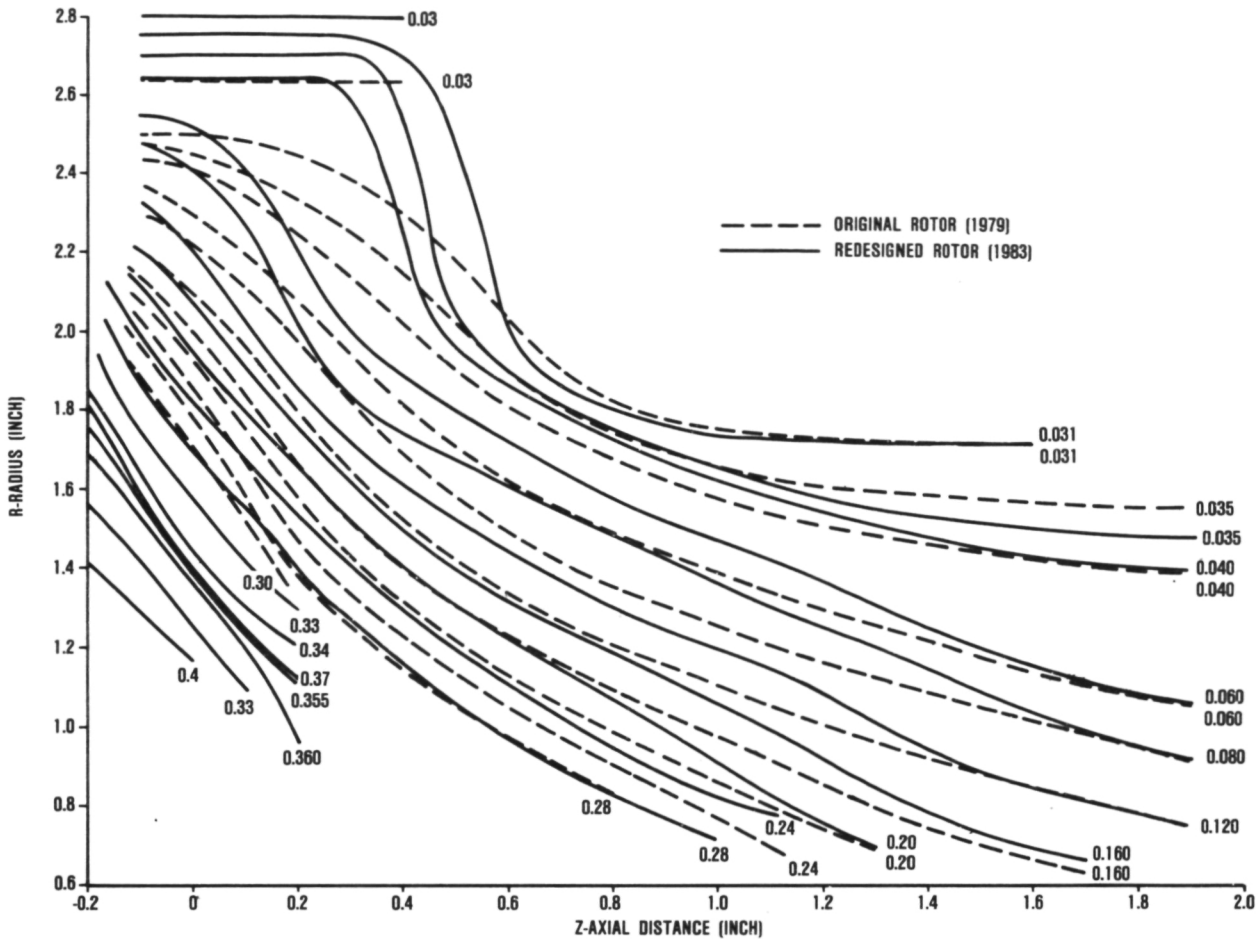

Figure 22. Comparison of Normal Thickness Distribution Between Baseline Rotor (1979) and Redesigned Rotor (1983).

ature conditions for the AGT101 varies between 1647-1940°F, and at these levels heat soak into the fuel nozzle can precipitate coking. To prevent this, air cooling has been incorporated into the Simplex design. In addition, air assist, is used to enhance fuel atomization.

The fuel nozzle was computer modeled for heat transfer analysis to determine the range of fuel passage surface temperatures for several configurations. This data is presented in Table 5. Isotherms for selected fuel nozzle configurations are shown in Figures 28 through 31. The environmental conditions correspond to rig simulation of engine idle with a suppressed temperature (1600°F versus 1940°F). The most significant configurations are those that incorporate film cooling on the upstream and downstream sides of the fuel distribution ring, configurations 5-8. This technique reduces the surface temperature from approximately 500°F to approximately 285°F or lower, and thus enhances nozzle survivability characteristics.

Based on this analysis, a modified Simplex fuel nozzle depicted in Figure 32 is being manufactured by Delavan Corporation. The nozzle configuration retains the same outer envelope as the original Simplex Nozzle.

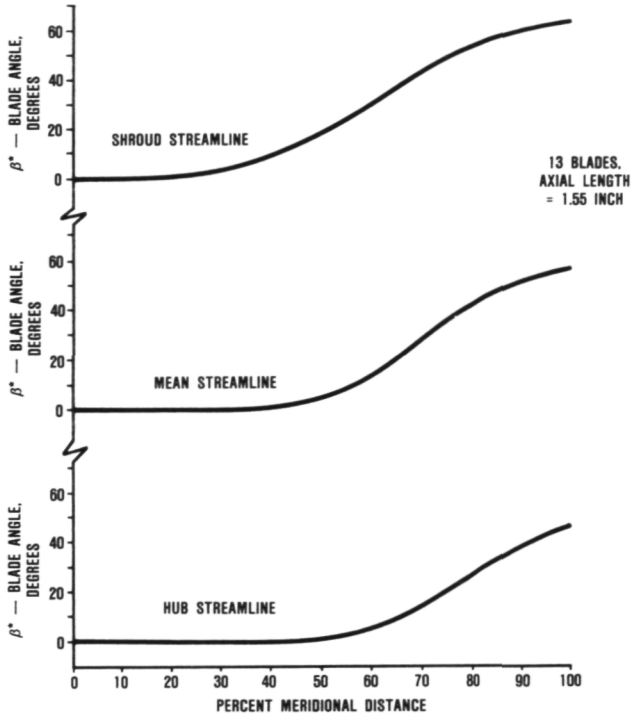

Figure 23. Turbine Rotor Blade Angle Distribution.

However, the modified nozzle separates the fuel distributor ring from the main nozzle body via an air plenum, and both the upstream and downstream faces are film cooled. Additionally, the fuel injection orifice diameters have been increased from 0.012 to 0.018 inches for greater particle tolerance.

4.4 Regenerator

4.4.1 Ford Regenerator Development

4.4.1.1 Regenerator Cores

Two additional thick-wall CO-3 material cores (GE-Cordierite coated and impregnated) were purchased from NGK during this report period. This combination has produced core porosity leakage equivalent to the Corning cores. In addition, an order was placed for three Corning thin-wall cores.

As stated in Reference 6, NGK must develop a dense MAS material to fabricate cores having thin-wall (0.0030 inch), high cell density (1500 cells per square inch) and an

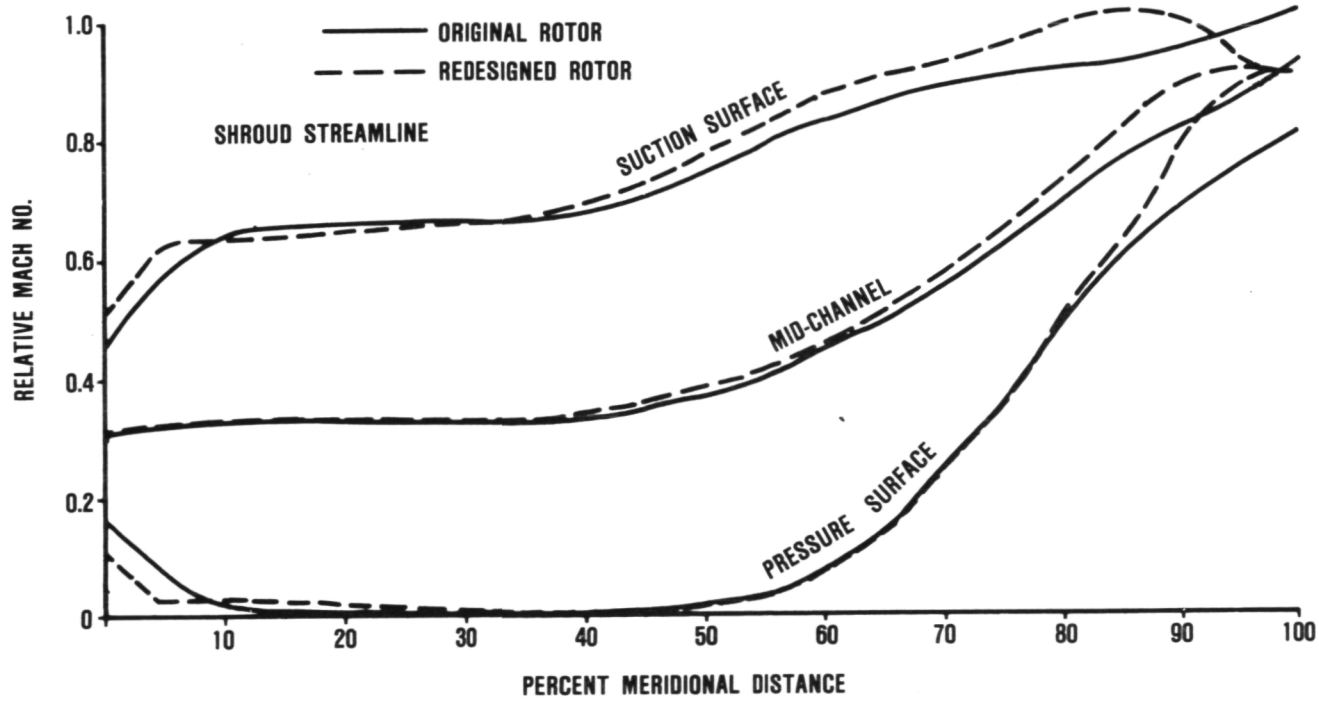

Figure 24. AGT101 Rotor Surface Velocity Distribution (Shroud).

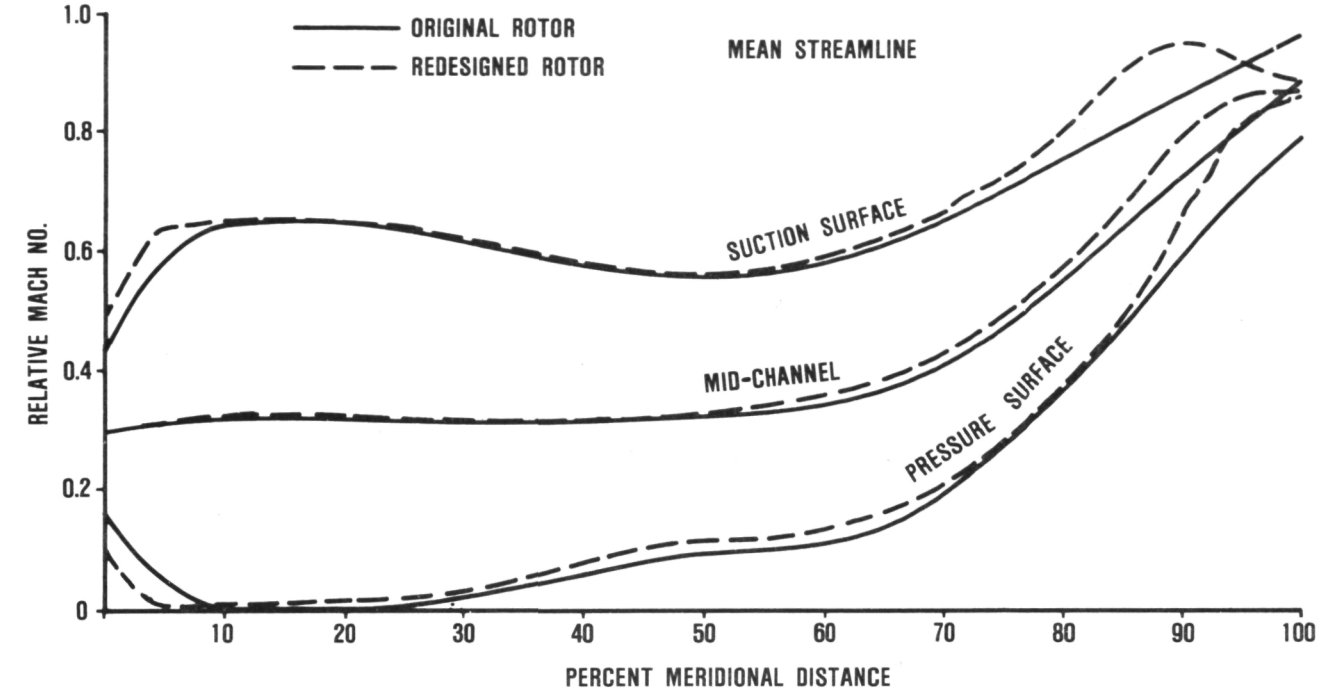

Figure 25. AGT101 Rotor Surface Velocity Distribution (Mean).

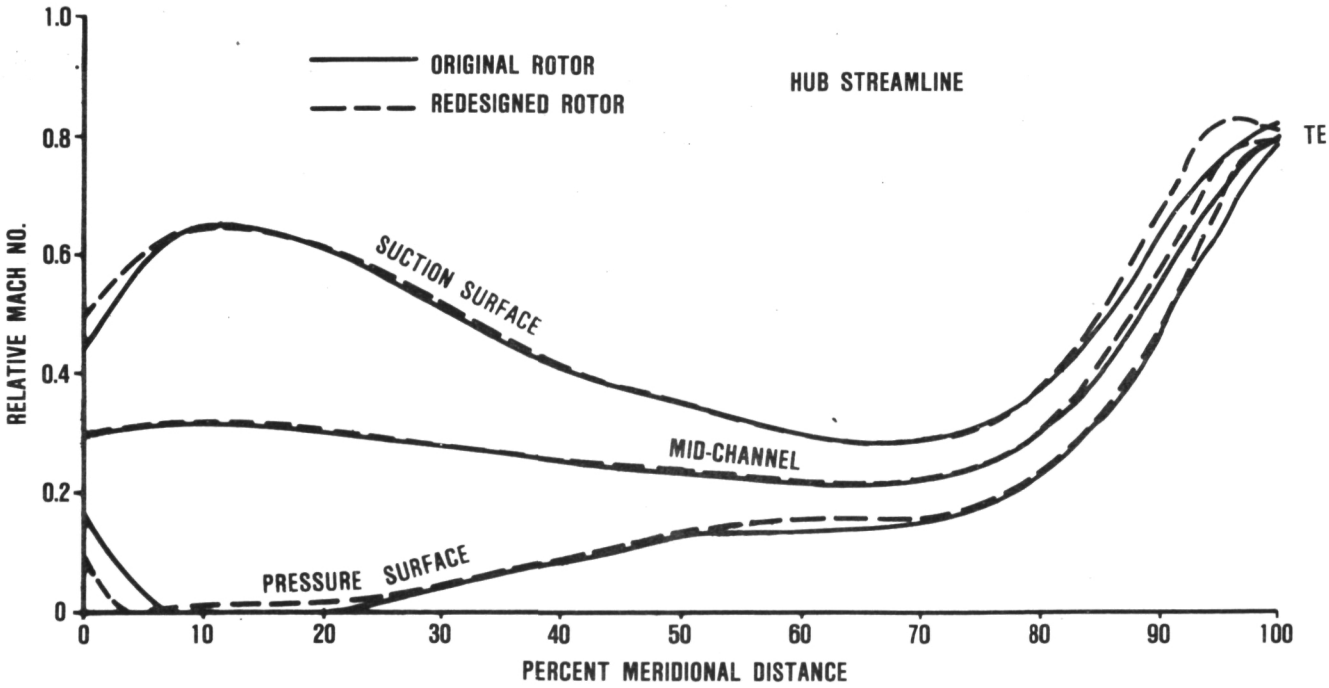

Figure 26. AGT101 Rotor Surface Velocity Distribution (Hub).

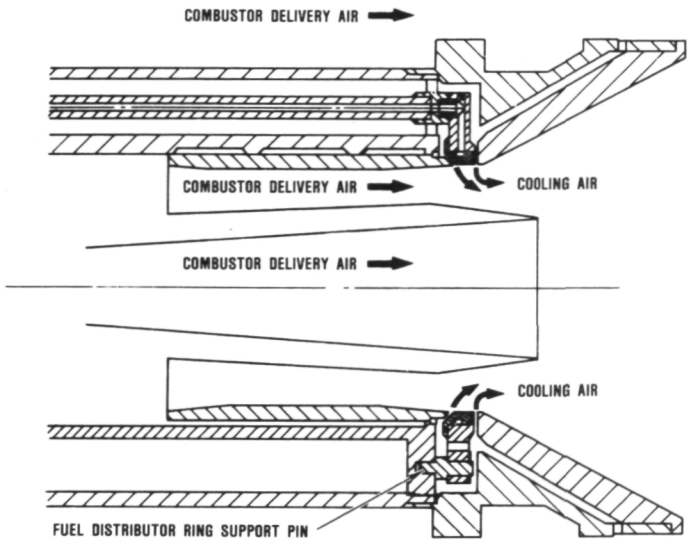

Figure 27. Simplex Fuel Nozzle.

isosceles triangular structure to meet the performance objectives for effectiveness and pressure drop. Due to the increased porosity leakage associated with this structure, a dense material is required.

As an interim solution, NGK is developing extruded rectangular cell matrices with cell densities of 1100 and 1380 cells per square inch with 0.0047 and 0.0042 inch wall thickness, respectively.

NGK expects the thru-wall leakage of these structures will be at an acceptable level with improvement in thermal efficiency when compared with the original 900 cells per square inch isosceles triangular matrix. A comparison of predicted performance for these matrices is listed on Table 6. Full-size cores with the extruded rectangular geometries are scheduled for the next report period.

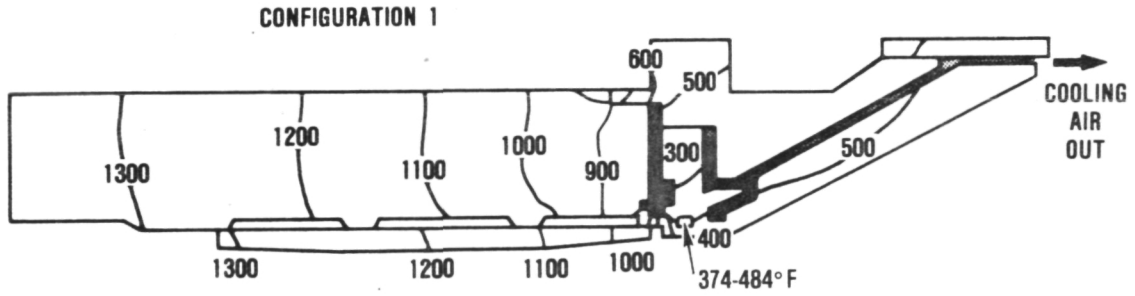

Figure 28. Simplex Fuel Nozzle Heat Transfer Analysis, Configuration 1.

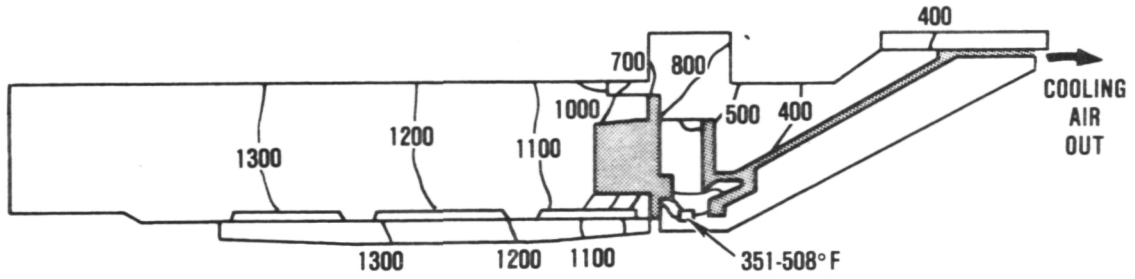

Figure 29. Simplex Fuel Nozzle Heat Transfer Analysis, Configuration 3.

TABLE 5. FUEL DISTRIBUTOR RING SURFACE TEMPERATURES FOR SIMPLEX MOD I FUEL NOZZLE

Conditions: Test rig simulation of engine idle

Combustor air inlet temperature = 1600°F
Combustor air inlet pressure = 25 psia
Fuel flow = 1.8 lb/hr
Fuel temperature = 100°F
Cooling airflow rate = 0.54 lb/min
Cooling air temperature = 80°F
Air assist temperature = 80°F

Configuration	Description	Air Assist, lb/min	Average HTC*	Temperature Range, °F	Figure
1	Simplex fuel nozzle (4.3-1)	0.03	400	374-484	28
2	As 1 but HTC decreased	0.03	38	428-553	
3	As 1 but with upstream plenum	0.03	38	351-508	29
4	As 3 but HTC increased and air assist flow increased	0.06	90	337-492	
5	As 1 but with film cooling effectiveness = 0.50	0.03	38	272-285	
6	As 5 but with film cooling effectiveness = 0.75	0.03	38	243-252	
7	As 5 but with increased air assist flow and increased HTC	0.06	90	234-245	30
8	As 7 but without yttria stabilized zirconia coating on inner and top surfaces	0.06	90	242-254	31

*HTC = Heat Transfer Coefficient

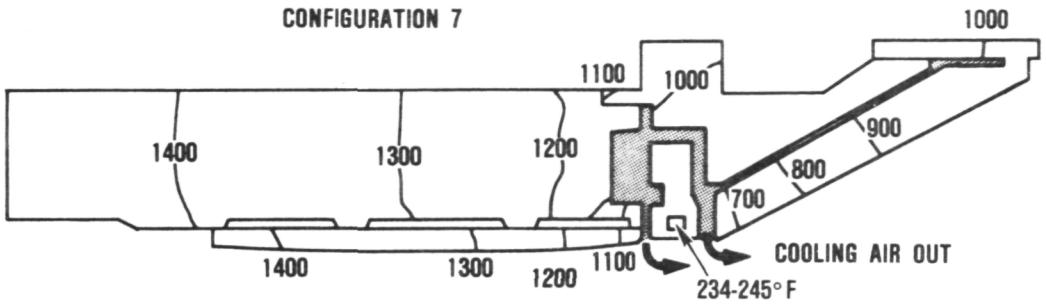

Figure 30. Simplex Fuel Nozzle Heat Transfer Analysis, Configuration 7.

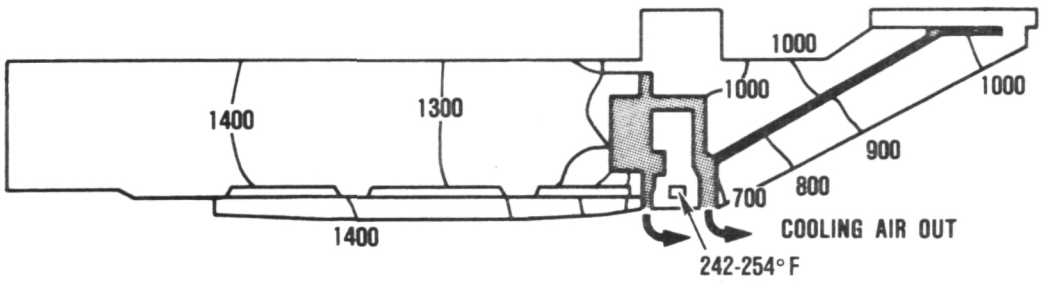

Figure 31. Simplex Fuel Nozzle Heat Transfer Analysis, Configuration 8.

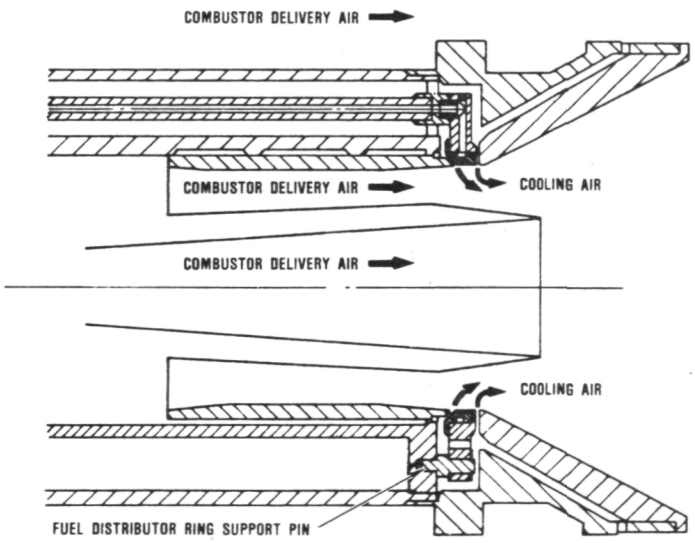

Figure 32. Modified Simplex Fuel Injector.

4.4.1.2 Regenerator Seals

The AGT regenerator seals are subjected to temperatures which cause the diaphragms to yield (Reference 6), and consequently lose the initial spring force which is vital to seal performance. Furnace tests were continued during this reporting period to determine the upper temperature limits of available materials for the ceramic engine, under simulated load conditions so that meaningful objectives can be made for diaphragm cooling as the final temperatures for AGT are approached.

In most cases, the maximum stress imposed on the regenerator seal diaphragms results from deflection due to clamping. Pressure forces therefore were not considered, but the deflection was controlled to normal working height, and also to bottomed out height where the core would rest on the retainer.

TABLE 6. REGENERATOR CORE PERFORMANCE

Objectives: (N_{GG} = 100 percent)

Effectiveness = 92.9-percent minimum
Pressure Drop = 7.5-percent maximum
Porosity Leakage = 0.5-percent maximum

	Wall Thickness, inch	Cell Density holes/inch^2	ε, percent	ΔP/P, percent	Leakage, percent
Corning-Wrapped Sinusoidal	0.0025	1310	91.9	7.3	0.20
NGK - Initial Extruded Isosceles	0.0055	920	90.1	6.0	0.30
NGK - Latest Extruded Isosceles	0.0030	1510	93.6	7.3	0.80
NGK - Latest Extruded Rectangular	0.0042 0.0047	1380 1100	93.3 91.4	9.2 7.2	0.50*

*Estimated

The tests (Reference 6) were continued for the AGT101 ceramic engine at 1600°F maximum material temperature goal for the cooled diaphragm. Material options included high temperature nickel base alloys such as Rene 41 and Waspaloy. When possible, different conditions of the same material were used. At ceramic engine conditions, both Rene 41 and Waspaloy have a yield strength of approximately 75,000 psi after precipitation hardening. Test specimens were made to the standard crossarm configuration which is a single element folded and formed as shown in Figure 33. This configuration is free of welds and any other process that might affect the material condition. Test results show that when the materials satisfactorily perform, the stress levels are sufficiently below the 75,000 psi level. Based on the furnace tests and

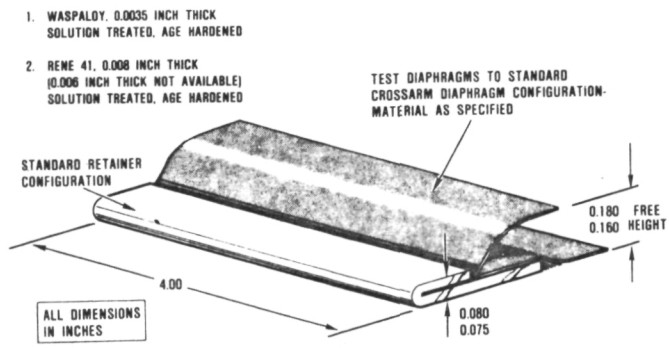

Figure 33. Regenerator Seal Material Test Specimen Configuration.

analysis, an acceptable stress level can be maintained provided the core is not bottomed out on the retainer.

To accommodate the higher operating temperatures associated with the ceramic engine, the regenerator inboard (hot) seal crossarm will require diaphragm cooling. The main emphasis during this reporting period has been design of the initial cooled diaphragm seal, designated as Phase 4, and illustrated on Figure 34. By incorporating a funnel in the secondary diaphragm attached to the ends of the crossarm, compressor discharge air is allowed to flow along the entire length and then vented into the regenerator high pressure exit air stream as shown on Figure 34.

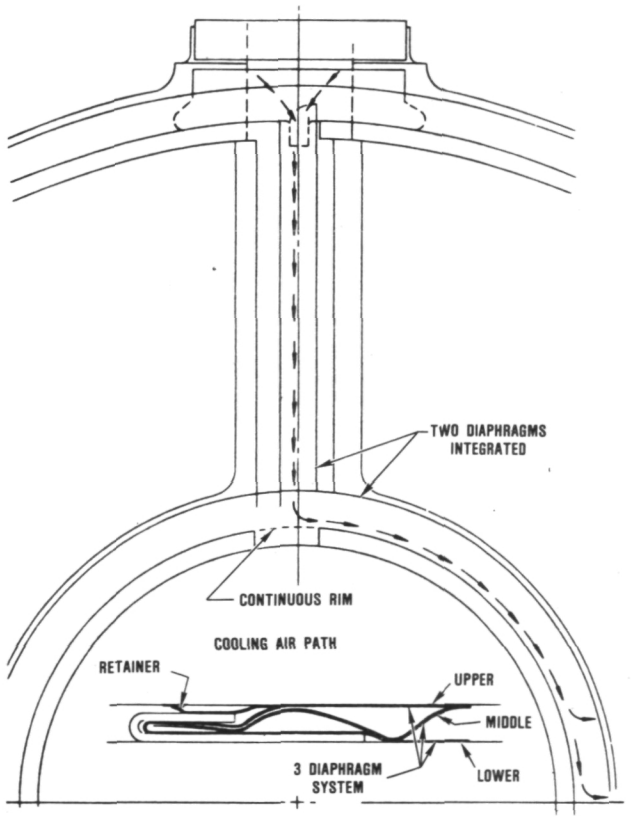

Figure 34. Cooled Regenerator Seal Schematic, Phase 4.

To limit the diaphragm material temperature to a maximum of 1600°F for ceramic engine conditions, the amount of cooling air flow must be determined by iterative test and analysis. A computer program for three-dimensional heat transfer analysis is being utilized. The hot inboard seal diaphragm cooling analysis has been initiated. An initial inboard regenerator seal with provisions for diaphragm cooling was shipped to Garrett for evaluation in the hot structures rig.

The main objectives for the Phase 4 seal system were to preserve the leakage characteristics associated with the Phase 3 design with a reduction in mechanical load characteristics to reduce drive torque requirements. To supplement prototype hardware evaluations, the Phase 4 seal system was evaluated analytically utilizing a structural dynamics computer code (MENTOR II). By incorporating proper damping characteristics this program can determine diaphragm loads and stresses for a simulated structural analysis at specified clearances. For a diaphragm system with the lower, upper and retainer fabricated from 0.004 inch foil thickness, the Phase 4 system was analyzed with 0.004, 0.006, and 0.008 inch middle diaphragm thicknesses. Seal contact force at simulated installed and cruise operating conditions are listed on Figure 35 for the different diaphragm material combinations. For comparative purposes, the seal force characteristics for the Phase 3 design are included on Figure 35. Based on these results the load characteristics for the Phase 4 design can be reduced with respect to Phase 3 by proper selection of the middle diaphragm thickness.

Utilizing the analytical results as a guideline, prototype Phase 4 seals with different diaphragm thickness combinations were fabricated to measure mechanical load characteristics and static seal leakage.

Phase 4 seals have been tested in the static seal leakage rig with 0.004, 0.006, and 0.008 inch middle support diaphragm thicknesses. The mechanical load characteristics for each of these seals were measured. These load

DESIGN	DIAPHRAGM THICKNESS (INCH)				LOAD (LB/IN) AT SWH*	
	L	M	U	R	0.276 CRUISE	0.285 BUILD
PERIPHERY						
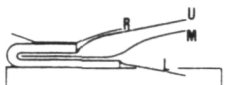	0.006	0.008	0.006	0.006	18.5	6.8
PHASE 3	0.003	0.008	0.003	0.006	13.0	4.3
	0.004	0.004	0.004	0.004	7.0	2.0
	0.004	0.006	0.004	0.004	10.0	4.3
PHASE 4	0.004	0.008	0.004	0.004	29.5	11.7
CROSSARM						
	0.004	0.004	0.004	0.004	15.7	7.5
PHASE 3	0.004	0.008	0.004	0.004	81.0	31.0
	0.004	0.004	0.004	0.004	8.0	1.5
	0.004	0.006	0.004	0.004	9.7	1.5
PHASE 4	0.004	0.008	0.004	0.004	21.0	4.3

* = SEAL WORKING HEIGHT

Figure 35. AGT Regenerator Seal Design Analysis.

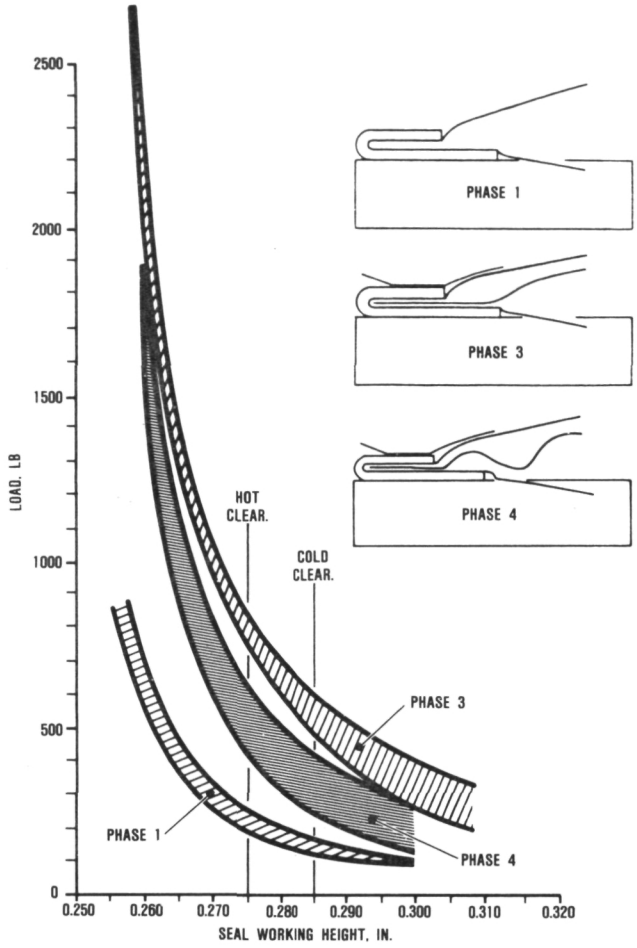

Figure 36. Seal Load Characteristics.

characteristics (Figure 36) indicate the Phase 4 design is an effective compromise between the Phase 1 and Phase 3 designs. The analysis correlates quite well with the actual hardware.

The hot (inboard) seal demonstrated a significant reduction in leakage for the 0.006 and 0.008 inch middle diaphragms. The cold seal exhibited a slight reduction. In general, the total leakage of the prototype Phase 4 seals is comparable to Phase 3. Note that the initial Phase 4 seals do not have the proper inside and outside corner secondary diaphragms at this time.

A controlled test sequence of the prototype Phase 4 seal in the static seal rig indicated that 80 percent of the total seal leakage is from the diaphragm system with the remaining 20 percent under the shoe. A similar study at Garrett supported this observation. The areas of relative leakage in the diaphragm system are indicated on Figure 37.

Since significant leakage reduction potential exists between diaphragm segments, spot or seam welding of the upper and middle diaphragms of a Phase 4 system will be evaluated. Previous seam welding of an upper and lower diaphragm for the Phase 1 system indicated slight leakage reduction at part power conditions.

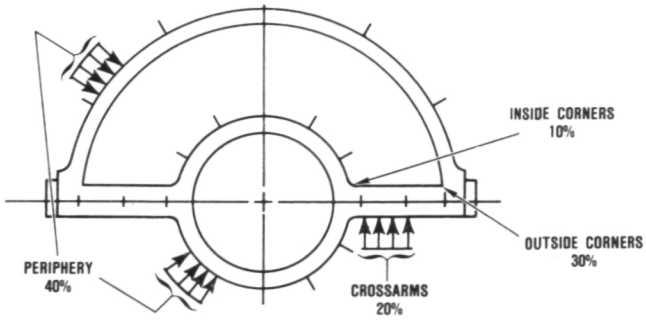

Figure 37. Areas of Relative Leakage in Diaphragm System.

To properly evaluate diaphragm design concepts, flat shoes are essential. New shoes made with the latest processing techniques, which includes stress-free cutting, have been ordered.

Test data and regenerator core and Phase 3 seal hardware inspection indicate the crossarm center hole region of the seals appear to be the main problem area for leakage and torque. A fixture has been designed that will attach to the cover bolt circle to incorporate dial indicators to measure the center hole regions of the flow separator housing and exhaust cover. This fixture will be available for the hot regenerator rig during the next report period. Seals are being fabricated for evaluation during the next report period. The main purpose of this test sequence is to determine the effect of adjusting seal system loads on core position and resulting leakage variation.

4.4.2 Garrett Regenerator Testing

During this reporting period, the hot regenerator rig testing was resumed with the purpose of defining the current state of AGT101 regenerator system development for the metal engine. Data that described core performance, discharge temperature distribution and regenerator seal leakage at idle and cruise conditions was collected. Included in this regenerator build were the following regenerator hardware:

- o Core: Corning AS, wrapped sinusoidal matrix, S/N FM.44.02
- o Hot Seal: Ford Phase III, Rene 41, seal diaphragms, S/N Hx-017
- o Cold Seal: Ford Phase III, Inco X-750 seal diaphragms, S/N CS-011

To evaluate the effect of regenerator pocket dimension (ie, seal working height) on seal leakage, the pocket dimension was changed after the first series of tests. The pocket dimensions were:

Original Build (Cold) - 3.875 inch
Revised Build (Cold) - 3.865 inch

Test conditions based on current metal engine operating conditions were selected. Test cell limitations restricted regenerator drive speeds to 15 rpm or less, and air flows to 30 lb/min or less. Rig inlet temperatures were 1200 and 250°F, for the LP and HP inlet, respectively. Regenerator leakage was measured using a helium leak detection apparatus.

Core performance and measured leakage are shown in Table 7. The core discharge gas temperature distribution, shown at cruise and idle on Figures 38 and 39, is based on the array of double shielded thermocouples positioned on the core LP and HP discharge faces. Note that over the range of flows and regenerator speeds tested, the thermal distribution on the HP discharge face of the core is very uniform.

The regenerator seal leakage was measured by seeding the HP inlet air with helium and comparing the concentration of helium in the LP discharge air with that at the HP discharge. All measurements were taken during rig operation with rotating regenerator and preheated rig inlet air to approximate metal engine operating conditions. This data is shown on Figure 40.

Of interest is that the slope of the leakage curve abruptly changes at seal differential pressures above 20 psid. This probably is due to a change in seal working height caused by pressure induced deflection of the flow separator housing support structure. Further, sim-

TABLE 7. SUMMARY OF AGT REGENERATOR PERFORMANCE

Airflow, lb/min	10	15	20	30
LP Inlet Temperature, °F	1200	1200	1200	1200
HP Inlet Temperature, °F	250	250	250	250
LP Inlet Pressure, psig	1	2	3.5	5
HP Inlet Pressure, psig	8	13	18	26
*Seal Leakage, percent (3.875 inch pocket)	11.2	9.7	8.2	7.4
*Seal Leakage, percent (3.865 inch Pocket)	8.1	6.7	6.6	6.3
HP Effectiveness	0.955	0.956	0.950	0.946
HP ΔP/P	0.0067	0.0059	0.0057	0.0041
LP ΔP/P	0.015	0.023	0.023	0.021

*Percentage of total rig HP flow

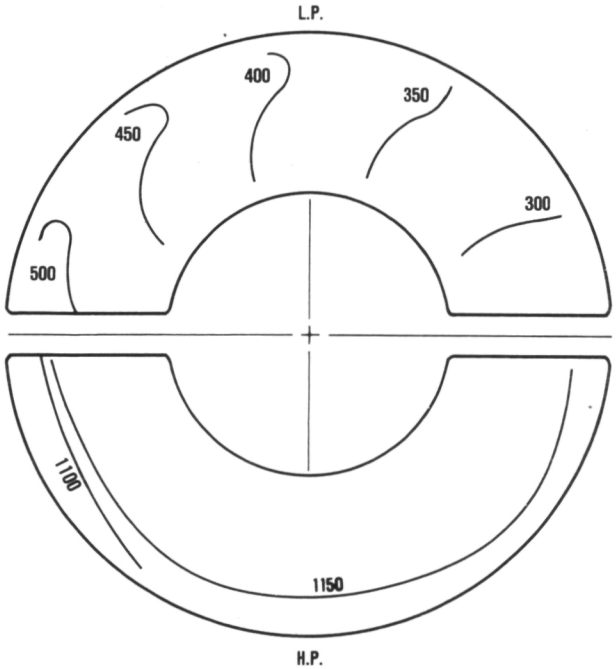

Figure 38. Core Discharge Gas Temperature at Cruise, °F.

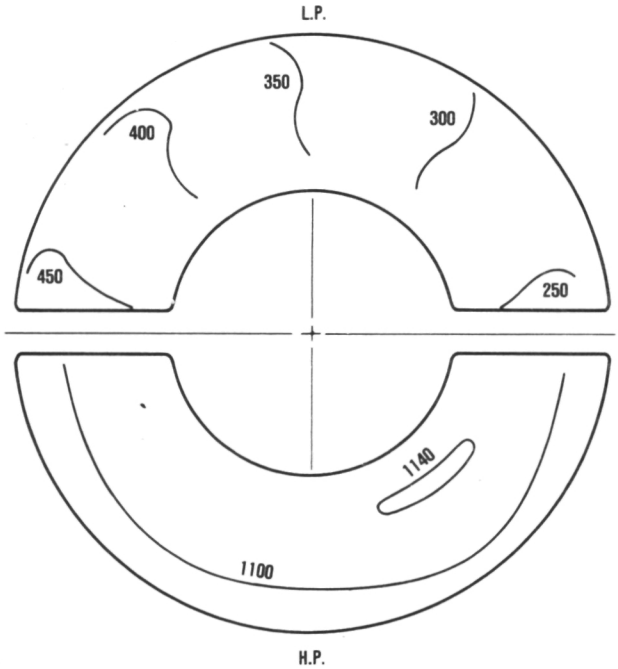

Figure 39. Core Discharge Gas Temperature at Idle, °F.

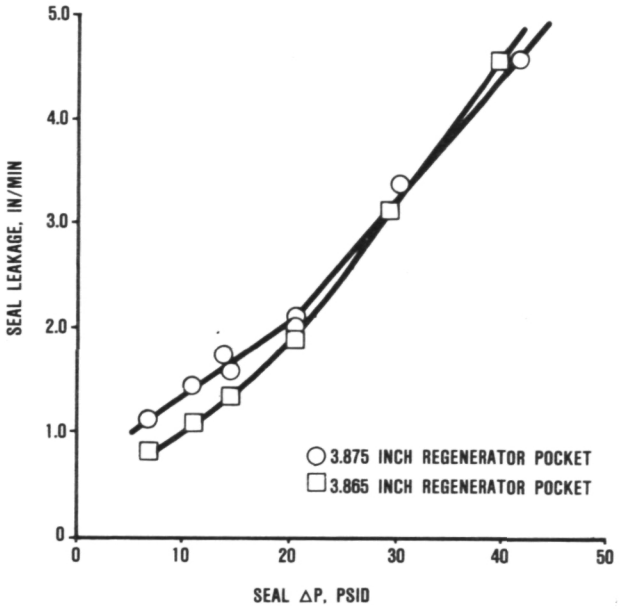

Figure 40. Regenerator Seal Leakage.

ilar deflections probably are present in the metal engine.

As the test was concluded the regenerator core became separated from its elastomer mounted ring gear. The separation occurred as high drive torques caused a pre-existing core delamination adjacent to the elastomer to propagate around the core perimeter. The excessive drive torques are particular to this rig and are associated with the contraction of the regenerator pocket due to thermal influences on the rig structure. Design is under way to substantially reduce the variation of the regenerator pocket due to both thermal and pressure influences for the rig and engine.

4.5 Ceramic Material

4.5.1 Component Design Improvements

The AGT101 ceramic development program utilizes an iterative design-fabrication-test approach to derive fabricable, low stress component designs. In this effort thermal and stress analytical evaluators have continued to be refined; and empirical component fabrication and testing results have been obtained. Results of both evaluations have provided sufficient information to perform the first overall design improvement for components that have proven to be difficult to fabricate or are highly stressed.

These "B" iteration design modifications initially were directed toward the inner and outer diffuser housing and the turbine shroud. These three components experience higher than desired peak stresses during light off transients, and have been modified for stress reduction. Additionally, where possible, design changes have been made to simplify component fabrication. These components are discussed in the following sections.

4.5.1.1 Turbine Shroud

Thermal stresses peak in the turbine shroud during light off when the inner gas path surfaces heat more rapidly than the outer regions. Additionally thermal gradients are produced along the turbine inlet and shroud contour surfaces due to the variation in heat transfer coefficients along the meridional flow path.

Stress reducing modifications to the shroud have included scalloping the outer flange region and varying wall thicknesses in proportion to the heat transfer coefficient variations. These changes are directed toward reducing the thermal gradient throughout the turbine shroud. The design changes are illustrated in Figure 41.

These design modifications have resulted in a predicted reduction in stress from 25.2 ksi to 16.2 ksi, a reduction of over 40 percent. The design changes have not significantly affected fabrication difficulty.

4.5.1.2 Inner and Outer Diffuser Housings

Thermal stresses in both the inner and outer diffuser housing also result from the radial thermal gradient created during light off. In both parts the inner portion heats more rapidly than the outer regions, producing the temperature variation. Additionally, the outer

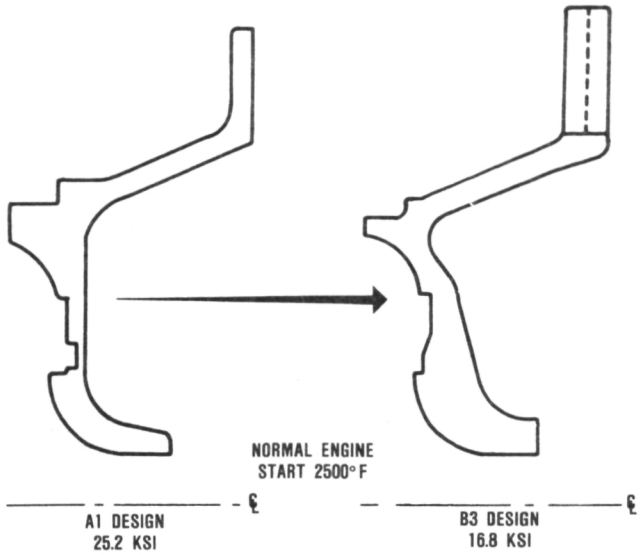

Figure 41. Turbine Shroud Design Evolution.

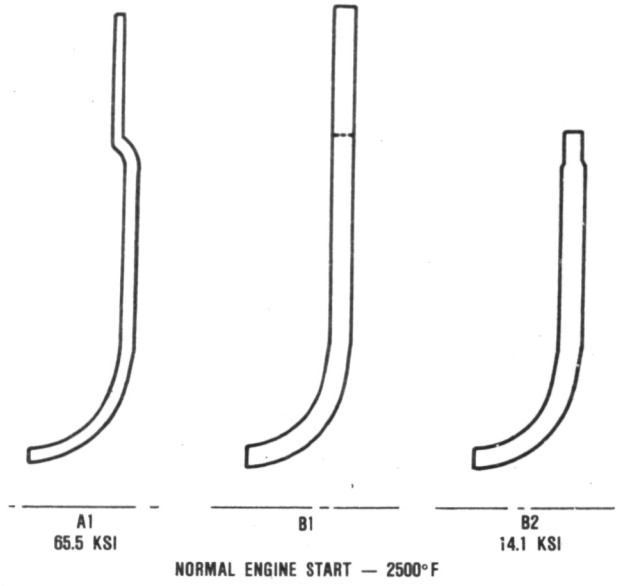

Figure 42. Outer Diffuser Housing Design Evolution.

diffuser rim slots and holes in the inner diffuser act as stress risers.

Design modifications to these components resulted in the "B" designs shown in Figures 42 and 43. As illustrated, both components have become simple, nearly flat plates without rim holes or slots. In addition to the stress reductions for the inner and outer diffuser housing, the design modifications have simplified the fabrication of these parts.

The "B" design inner diffuser has eliminated the outer gas flow path surface requiring that an additional part be utilized. The 2000°F gas temperature, lack of mechanical loading and the low peak gas velocity of 50 to 75 ft/sec may allow materials other than monolithic ceramic components to form this gas path surface. One material being investigated for use in this location is vacuum formed Al_2O_3 - S_1O_2 fiber insulation. (Babcock and Wilcox) Inc. The insulation will also fill the cavity between the turbine and compressor diffusers and will be coated with ceracote for strength where exposed to the turbine discharge gases for improved surface strength. A prototype ceramic fiber component is shown in Figure 44.

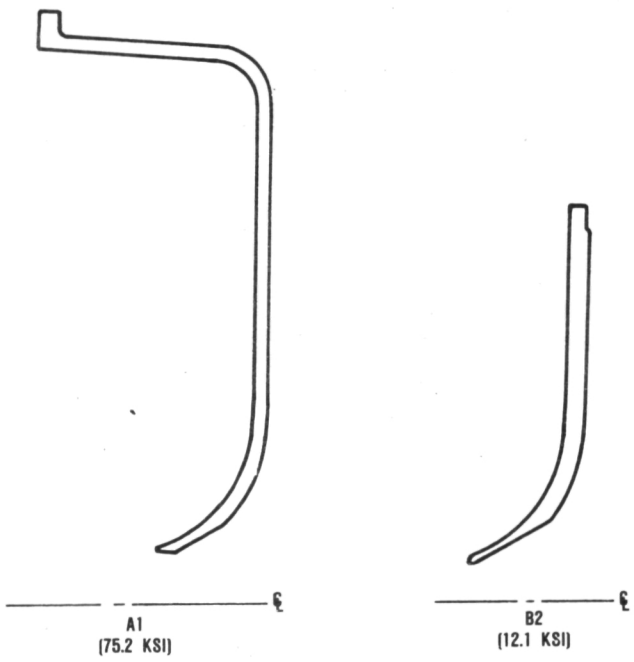

Figure 43. Inner Diffuser Housing Design Evolution.

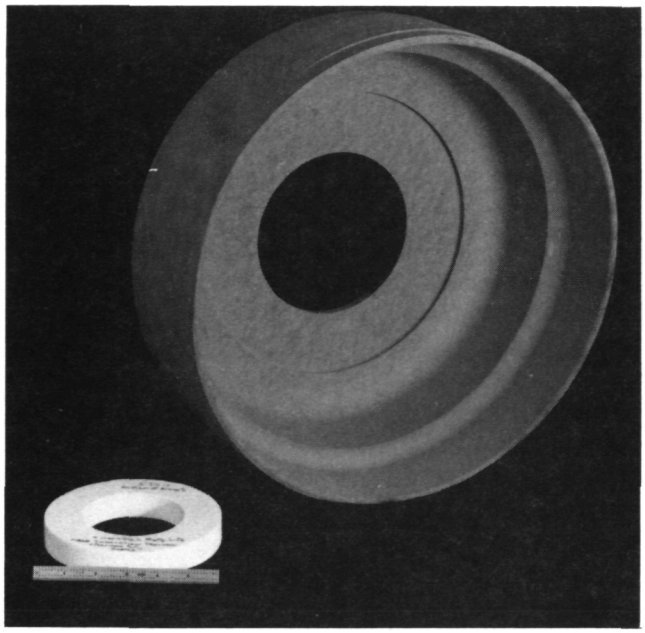

Figure 44. Prototype Ceramic Fiber Insulation (Vacuum Formed).

Initial tests of the insulation were conducted at 2000°F and 150 ft/sec gas velocity (twice maximum power velocity). Superficial cracking of the test piece was noted, however, no material loss was noted.

4.5.2 Materials

4.5.2.1 Ceramic Material Testing Summary

A summary of the material property results is presented in Table 8. Additionally, a material characterization reference chart, indicating where additional information (generated by Garrett) can be found, is presented in Table 9.

4.5.2.2 Heat Treated RBSN Data Base

Based on results discussed in previous reports, all RBSN components receive a flash oxidation heat treatment after final machining. In an effort to provide a basis for analytical stress analysis and probabilistic assessment of heat treated RBSN parts, flexure results obtained during several ACC RBSN 104 heat treatment and machining studies were compiled and analyzed as a group. Data included in this compilation includes results from room temperature tests on transverse ground, or as-nitrided test bar surface conditions with 2000°F exposures varying from 2 hours to 150 hours. Flexure results analyzed are summarized in Table 10, and the Weibull analysis is presented in Figure 45. As illustrated, the characteristic for these data is 54.8 ksi and the Weibull modulus is 8.5. Flexure strength values range from 39.7 to 63.2 ksi.

4.5.3 Ceramic Structures Rig Testing

Build 6 of the ceramic structures rig was initiated in January 1983. All hardware has been thermally and/or mechanically screened prior to initiation of the build. Table 11 provides a listing of the qualified components, materials, and suppliers. The test rig was assembled as shown in Figure 46. The transient selected was coordinated with the power section development group and agreed to as fully functional transient for engine operation.

The unit was installed in the test facility and testing initiated. Approximately 16 hours of testing was conducted with several acoustic emission signals above 85 db recorded. The occurrence of these signals were discussed during test with the cognizant test and acoustic engineers, and evaluated as non-critical signals. Following initial testing, the unit was shut down and it was decided to visually inspect the regenerator seals and the ceramic parts. On partial disassembly, Figure 47, it was noted that a catastrophic failure had occurred. The test rig was removed from the facility and a full disassembly initiated. Figures 48 to 51 depict the failed hardware.

Inspection during disassembly, revealed that the inner rim of the flow separator housing showed evidence of shear failure, ie, 45 degree shear plane, resulting from an axial load. Detailed review of the assembly and calculated stack measurements used for setting regenerator shield to flow separator

TABLE 8. SUMMARY OF AGT COMPONENTS AND MATERIALS.

Supplier	Material	Process	Condition	Qualification Bar							Ceramic Component						
				Room Temperature			Elevated Temperature				Room Temperature			Elevated Temperature			
				σ_θ [4]	M	Population	σ_θ [4]	M	°F	Population	σ_θ [4]	M	Population	σ_θ [4]	M	°F	Population
ACC																	
Inner Diffuser	RBSN	Slip	As-Fired	49.7	4.5	30	52.1	10.1	2200	10	44.3[6]	8	21	--	--	--	--
Outer Diffuser	(RBN104)	Cast	Longitudinally Ground	53.2	5.5	10					46.3	5.3	27	--	--	--	--
Turbine Shroud			Heat Treated	54.8	8.5	29											
ACC																	
Stator	RBSN (RBN124)	Injection Molded	As-Fired[1]	40.1	4.8	19	44.5	8.4	2200	23	--	--	--	--	--	--	--
ACC																	
Rotor	Sintered Si_3N_4 (SNN 502)	Slip Cast	Longitudinally[2] Ground	--	--	--	--	--	--	--	60.7[3]	18.5	24	--	--	--	--
	Sintered Si_3N_4	Injection Molded	As-Fired	89.2	8.9	30	80.9	7.6	1880	9	--	--	--	--	--	--	--
	(SNN 522)						66.1	11.1	2000	30							
							67.5	10.8	2200	10							
							25.6	13.6	2500	12							
Carborundum																	
Turbine Shroud, Stator	Sintered α-SiC	Injection Molded	As-Fired	48.6	9.5	30	45.0	5.0	2500	10	55.4[5]	7.1	9	--	--	--	--
Combustor Baffle	Sintered α-SiC	Slip Cast	Longitudinally Ground	49.4	5.8	30	41.4	6.7	2500	10	53.0	7.3	9	--	--	--	--
Transition Duct, Regen Shield, Back-shroud	Sintered α-Sic	Isopressed	Longitudinally Ground	57.7	7.7	30	56.2	11.9	2500	10	--	--	--	--	--	--	--
Ford																	
Rotor	SRBSN (RM-2)	Slip Cast	Longitudinally Ground	109.3	19.8	6	73.1	16.4	2200	6	--	--	--	--	--	--	--
Stator	RBSN	Injection Molded	As-Fired	43.1	9.2	39	45.8	7.7	2200	10	--	--	--	--	--	--	--
NGK																	
Backshroud, Transition Duct	Sintered Si_3N_4 (SN-50)	Isopressed	Longitudinally Ground	87.6	10.5	10	47.1	13.6	2000	7	--	--	--	--	--	--	--

All test bars 0.250 x 0.125 inch cross section unless noted. Bars tested in 4-point flexure, 1.50 inch outer span and 0.75 inch inner span. Cross head speed, 0.02 inch/minute

(1) Test bar cross section 0.31 x 0.15 inch

(2) Test bar cross section 0.2 x 0.1 inch

(3) 95 percent dense

(4) Characteristic strength, ksi

(5) As machined, longitudinally ground

(6) Test bar cross section 0.236 x 0.1 inch

housing preload was in error. This resulted in an insufficient gap to allow for differential thermal expansion between the metallic structural members and the ceramic components. Thus, as the metallic components thermally expanded, an excessive load was imposed on the flow separator housing resulting in fracture. This is the primary failure mechanism and all other damage as discussed in Section 4.5.3.1 is a result.

The assembly procedures and rig design have been reviewed and modifications incorporated as follows:

- Detailed inspections during the buildup of rig to correlate design intent
- Removal of the wave washer axial loading mechanisms in favor of a spring loading mechanism (engine system)

Additional hardware is being screened for build into the structures rig.

4.5.3.1 Structures Rig Build 6 Failure Analysis

Teardown of the structure rig build indicated several damaged components, as summarized in Table 12. Components were individually examined by visual and by 10-30X microscopy to assess fracture origins. Components were evaluated for fracture origins, and

TABLE 9. SUMMARY OF AGT CERAMIC MATERIAL CHARACTERIZATION AT GARRETT

	AiResearch Casting Co.				Carborundum Co.							Corning	Ford Motor Co.			NGK Locke	Pure Carbon
	Reaction-Bonded Si_3N_4		Sintered Si_3N_4		Sintered SiC			Reaction-Sintered SiC				LAS	SRBSN	RBSN	LAS		
	SC	IM	SC	IM	SC	IM	IP	CP	CM	IP	Hot Pressed SiC		SC	IM		IP	IP
	RBN-104	RBN-124 RBN-126	SSN-502	SSN-522					KX-01	KX-02			RM-2			SN-50	Refel
Flexure Strength																	
Room Temperature	S1-245 S7-S6-96	S1-251	S3-46	S1-256	S2-61 S6-97	S1-266 S6-99	S1-265	S1-264 S2-59				S6	S4-28	S2-68	S6		
Elevated Temp. T_1 (1800-2000°F)		S1-251		S1-256				S1-264	S3-51	S4-25		S6			S6	S3-45	
T_2 (2200°F)	S1-245			S1-257				S2-59 S1-264					S4-28	S2-68			
T_3 (2500°F)	S1-245	S1-251		S1-258	S2-61	S1-266	S1-265	S2-59 S1-264						S2-68			
Transverse Machined	S1-248			S1-255				S2-58 S1-277									
Longitudinal Machined	S1-248			S1-255		S1-266		S1-277	S3-51	S4-25			S4-28			S3-45	S3-48
Cut from Components	S4-24 CCM81		S3-46 S4-24				S2-87				S3-49						S3-48
Post-Machining Oxidation	S1-248				S2-61			S2-59 S1-277		S4-25							S3-48
Oxidation																	
Gradient Furnace				S4-30									S4-30				
Dynamic Durability Rig	*							*					S4-28				*
Stress Rupture																	
Static, Air			S6-	S4-31 S1-262 S2-63									S4-31				
Dynamic, Gas Fired	S2-65							S2-65									
Interface Considerations																	
Compatibility Test	S5-38 CCM82				S5-38 CCM82	S5-38 CCM82		S5-38 CCM82	S5-38 CCM82			S5-38 CCM82				S5-38 CCM82	
Sliding Tests	S2-74 S1-281							S2-75									
Coating Development	S2-78 S1-280							S2-78									
Shrink Fit/ Ratchet Tests																	
Thermal Shock (Stators)		S4-35				S4-35											
Spin Test (Rotor)																	
Bladeless Rotor			S3-46			S2-85	S2-85						CCM81				S3-48
Bladed Rotor			S5-35										CCM82				

*Tested under NASA 3500-Hour Durability Program, Contract DEN3-27.

SC = Slip Cast
IM = Injection Molded
IP = Isopressed
CP = Cold Pressed (Uniaxial)
SRBSN = Sintered Reaction Bonded Si_3N_4

Examples of Refereoces:

S1-245 = Page 245, First Semi-Annual Report

CCM82 = Paper presented at 1982 CCM

TABLE 10. SUMMARY OF HEAT-TREATED RBN 104 FLEXURE STRENGTH DATA

Test Bar Condition	Strength (ksi)
Transverse Ground and 2000°F/2 Hrs	57.0 58.7 56.2 55.9 43.4 63.2 52.1 43.2 48.1
As-Nitrided and 2000°F/2 Hrs	56.2 60.8 58.5 49.0 43.8 59.0 59.9 57.9
As Nitrided and 2000°F/50 Hrs	40.6
As Nitrided and 2000°F/150 Hrs	49.0 39.7 51.3 54.1 45.5 49.0 46.1 59.3 55.6 40.3 50.1
Characteristic Strength	54.8
Weibull Modulus	8.5

Flexure results obtained at room temperature. Test bar cross section: 0.250 x 0.125 inch. Four point flexure with outer span of 1.5 and inner span of 0.75 inch. Cross head speed: 0.02 in/min.

TABLE 11. CERAMIC STRUCTURES RIG, BUILD 6

Part Name	Supplier	Material	Quantity
Regenerator Core	NGK-Locke	MAS	1
Regenerator Shield	Carborundum	SASC	1
Transition Duct	Carborundum	SASC	1
Combustor Baffle	ACC	RBSN	1
Turbine Backshroud	NGK-Locke	SSN	1
Turbine Stators (Segmented)	ACC	RBSN	19
Turbine Shroud	ACC	RBSN	1
Outer Diffuser	ACC	RBSN	1
Inner Diffuser	ACC	RBSN	1
Flow Separator Housing	Corning	LAS	1
Rocker (Alignment Spacer)*	Norton/Garrett	HPSN	3
Eccentric Spacer*	Norton/Garrett	HPSN	3
Bolt, Turbine Shroud*	Norton/Garrett	HPSN	3
Contact Washer, Upper*	Norton/Garrett	HPSN	3
Contact Washer, Lower*	Norton/Garrett	HPSN	3
Crowned Washer*	Norton/Garrett	HPSN	6
Seal, Lower-Turbine Shroud (OD)*	Corning/Garrett	LAS	1
Washer, Wave Spring*	ACC/Garrett	RBSN	1
Seal, Upper-Turbine-Regenerator Shield (ID)	Pure Carbon	RSSC	2
Seal, Thermocouple-Flow Separator Housing (Spherical)*	Norton/Garrett	HPSN	4
Load Spacer-Inner Seal, Thermocouple*	Norton/Garrett	HPSN	1
Spacer, Thermocouple*	Carborundum/Garrett	SASC	5
Seal, Thermocouple-Transition Duct (Spherical)*	Carborundum/Garrett	SASC	2
Bushing, Thermocouple-Transition Duct*	Carborundum/Garrett	SASC	1
TOTAL COMPONENTS IN ASSEMBLY			67

*Material supplied/machined by Garrett

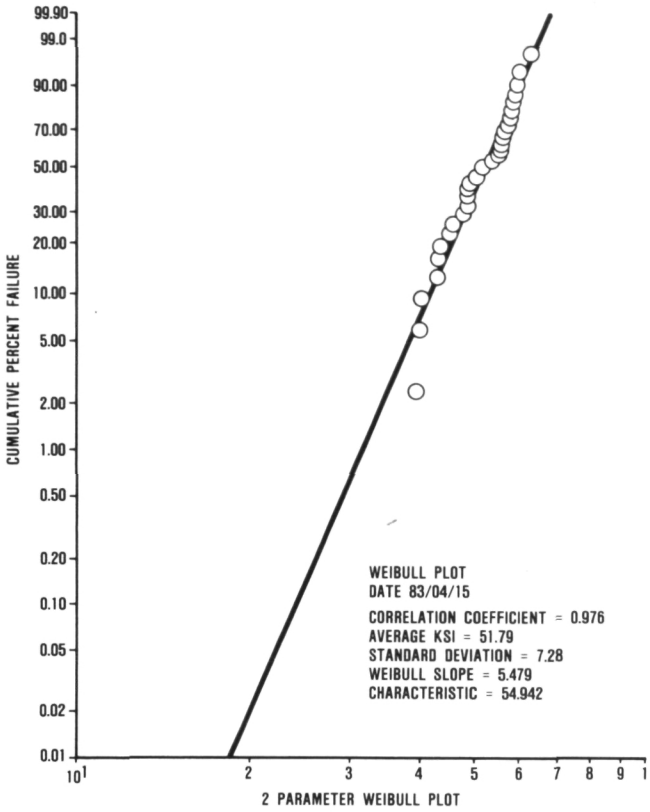

Figure 45. Weibull Plot for Composite.

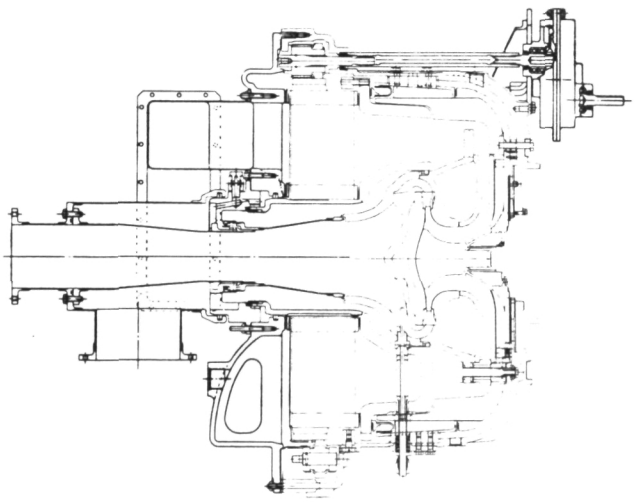

Figure 46. Ceramic Structure Rig.

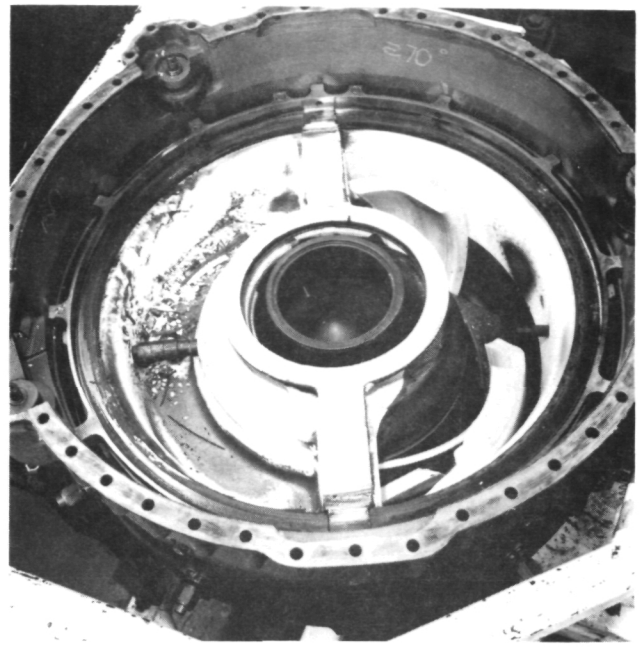

Figure 47. Initial Disassembly of Structures Rig, Build 6.

Figure 48. Structures Rig, Build 6 Transition Duct.

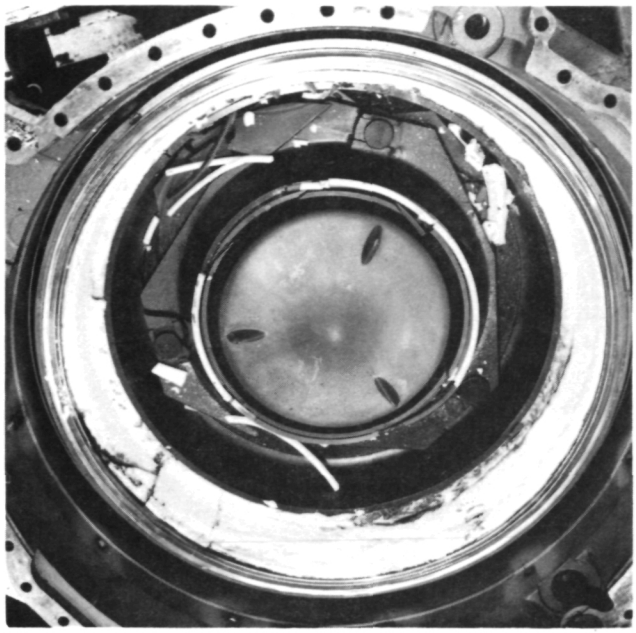

Figure 49. Structures Rig, Build 6 Combustor Baffle and Seal Rings.

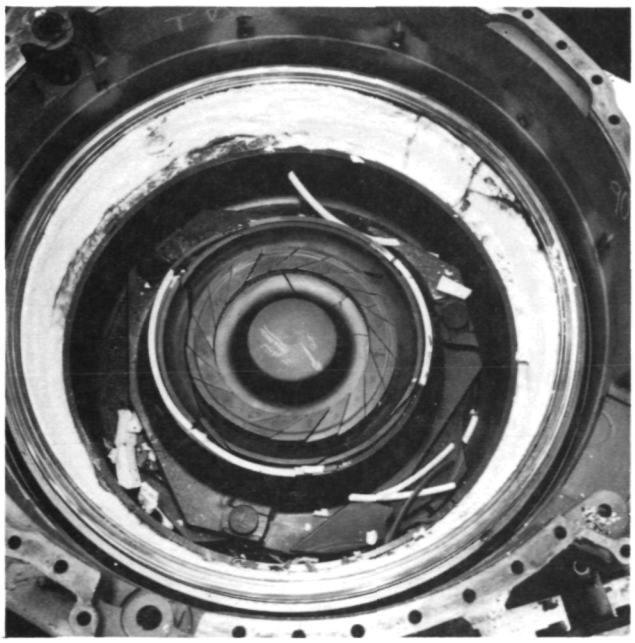

Figure 50. Structures Rig, Build 6 Stators and Turbine Shroud.

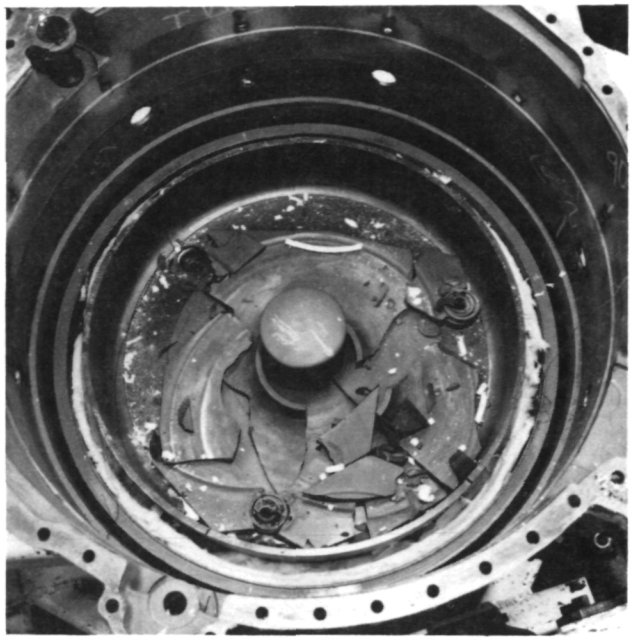

Figure 51. Structures Rig, Build 6 Inner and Outer Diffuser Housings.

estimates were made as to the mode of fracture, ie, mechanical loading, contact stress or thermal stress. Modes of fracture were analyzed based on the characteristics of the fracture surfaces including Walner lines, hackle marks and overall pattern of the fracture surfaces, as well as the type of mechanical and thermal stress distribution anticipated (or possible) under the known test conditions.

A summary of this analysis for the major ceramic components is presented in Table 13. Photographs of the components listed in the table also are illustrated in Figures 52 through 56. As indicated in these summaries, the primary mode of fracture is due to mechanical loading. No fracture causing material defects were identified at the fracture origins. Fractures thus were attributed to the stress states induced during the rig test.

Fracture characteristics on the flow separator housing indicate that this component was highly loaded in the axial direction on the

TABLE 12. STRUCTURES RIG BUILD 6 TEARDOWN SUMMARY

Damaged	Undamaged
Regenerator Core (AS)	Regenerator Shield (SASC)
Flow Separator Housing (LAS)	Transition Duct (SASC)
Turbine Shroud Seals (LAS)	Stator Set (RBSN)
Wave Spring (RBSN)	Backshroud (SN-50)
Turbine Shroud (RBSN)	2 Bolts (NC-132)
Combustor Baffle (1 Strut) RBSN	1 Eccentric Spacer (SASC)
Outer Diffuser (RBSN)	3 Rockers (NC-132)
Inner Diffuser (RBSN)	$T_{4.1}$ Support System (SASC)
Load Spacers (NC-132)	
1 Bolt (NC 132)	
2 Eccentric Spacers (SASC)	

TABLE 13. FRACTURE ANALYSIS SUMMARY, STRUCTURES RIG BUILD 6

Component	Fracture Origin	Fracture Cause
Flow Separator Housing S/N 14	Forward Outer Diffuser and regenerator shield step	Mechanical loading, ie, high axial load
Turbine Shroud S/N 185	Bolt hole and rocker Slot fillet	Mechanical loading, ie, high axial load
Outer Diffuser S/N 244	Contact zone for eccentric spacer	Mechanical, ie, contact stress
Inner Diffuser S/N 173	Bolt holes	Mechanical at contact region, and thermal from bolt hole
Combustor Baffle S/N 219	Strut tip	Contact stress

Figure 52. Flow Separator Housing, S/N 14.

Figure 54. Turbine Shroud, S/N 180.

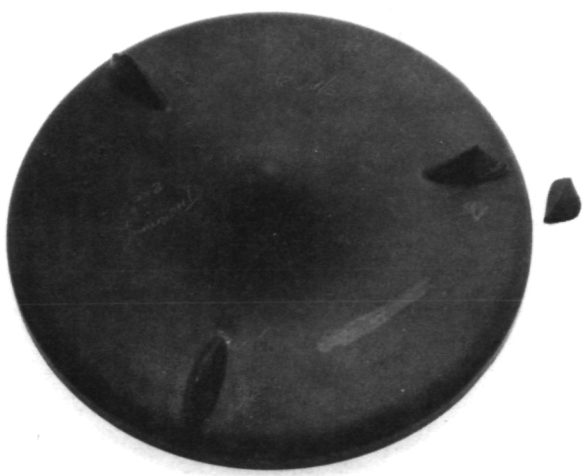

Figure 53. Combustor Baffle, S/N 219.

Figure 55. Outer Diffuser, S/N 244.

Figure 56. Inner Diffuser, S/N 173.

regenerator shield step. Likewise, damage to the combustor baffle and turbine shroud appears to have resulted from axial loading. In the flow separator housing, the axial load resulted in fracture of the regenerator shield step, with cracks propagating along the inner conical portion and radially to the outer rim. Fracture also initiated in the flow separator housing at the forward outer diameter of the cross-arm support. This fracture branched and travelled aft through the cross-arm as illustrated in Figure 52.

Fracture of the combustor baffle, Figure 53, occurred at one strut location. This damage was a result of axial loading and contact damage at the strut tip.

Turbine shroud damage initiated at bolt locations 2 and 3, as shown in Figure 54. Fractures initiated in the bolt hole and rocker slot respectively, due to excess axial mechanical loading.

Damage to the outer and the inner diffusers initiated at the bolt slots. In both cases, fractures initiated at contact locations where the diffuser surfaces contact the piloting eccentrics and rockers. Damage to the outer diffuser appears to be solely mechanical, whereas inner diffuser damage has mechanical and thermal stress contributions.

Damage to the remaining ceramic components appear to be secondary resulting from a shift in the structural load path, which occurred after the primary fractures of the parts discussed.

4.5.4 Hot Turbine Testing

After initial checkout (Reference 6), the hot turbine rig (Figure 57), was reassembled with an ACC silicon nitride turbine wheel, which had been cold spun to 80,000 rpm. Three cycles of operation in the rig were completed. The cycle included stabilization of speed at 60,000 rpm with 800°F inlet temperature, shutoff fuel to burner, hold speed at 60,000 rpm by increasing air pressure, and allow cooldown to below 400°F. This cycle imposed stresses in the ceramic wheel that were 2 to 3 times more severe than would be expected in a normal shutdown cycle when operated in the 1600°F metal engine. A picture of this wheel in the rig with the transition duct and nozzle assembly removed is shown in Figure 58. Inspection after disassembly revealed no damage or signs of distress to the ceramic components. As a result of this testing, this part could be used in a metal engine restricted to 80,000 rpm.

A second ACC silicon nitride turbine wheel was received and cold spun to 115,000 rpm. A three-dimensional finite element analysis of the stress fields in this part was performed assuming a "worst case" condition for a 1600°F engine operation. This situation was a combustor flameout while operating at 100,000 rpm at full load. The stress distribution is shown as Figure 59. A hot rig cycle that would subject the wheel to essentially identical stresses was defined. A typical example of this cycle is shown as a multi-

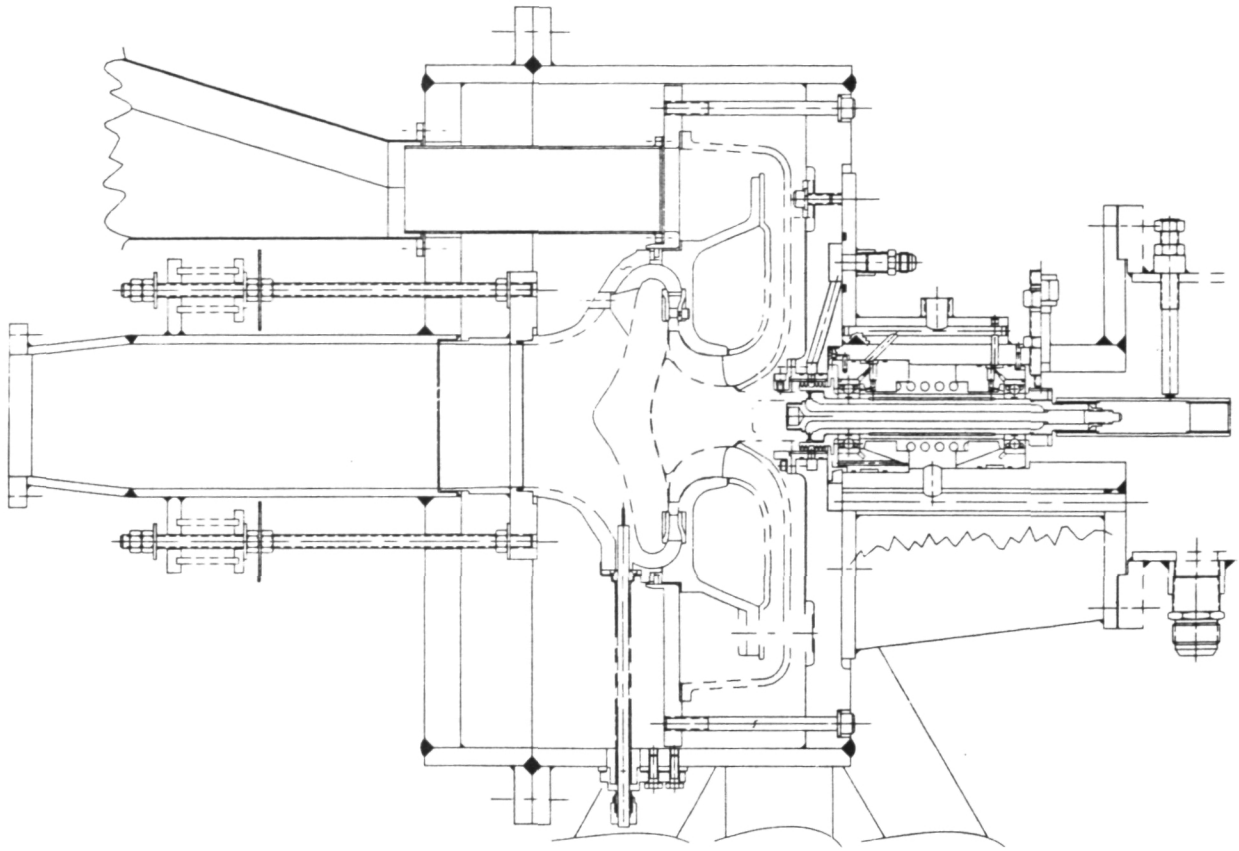

Figure 57. Hot Turbine Test Rig.

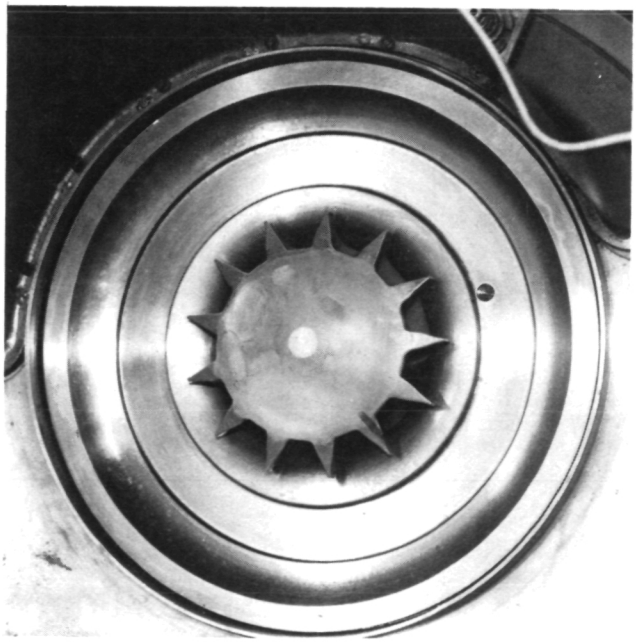

Figure 58. ACC Si_3N_4 Turbine Wheel Installed in Test Rig.

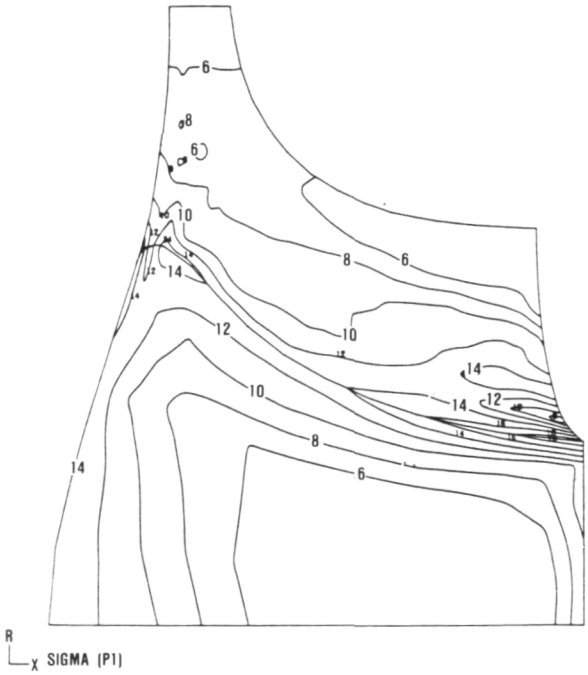

Figure 59. ACC Si_3N_4 Turbine Blade Stress Field, "Worst Case" Condition.

channel data recording (Figure 60). Manual control of the inlet pressure results in a speed droop when burner heat input is terminated; However, restoration of rig speed is rapidly accomplished. Three cycles of this operation were accomplished on the turbine wheel. Inspection after teardown, showed no evidence of any cracking, rubbing, or other distress on the turbine wheel. A picture of this turbine wheel is shown in Figure 61.

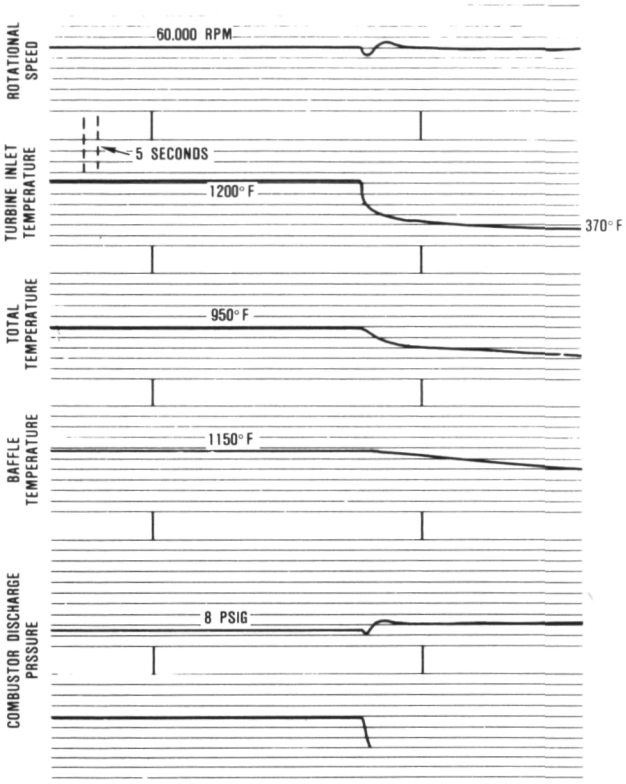

Figure 60. Multichannel Recording of Thermal Stress Cycle.

As a result of cold spin testing and thermal cycling, this wheel is considered satisfactory for use in a 1600°F engine without speed restrictions.

4.5.5 Turbine Attachment

A single wall sleeve is being evaluated for the ceramic rotor. The single sleeve coupling utilizes the shrink fit concept and non-ratchet design features of the dual sleeve. However, since the shrink fit concept is retained, a distorted outer diameter will occur during

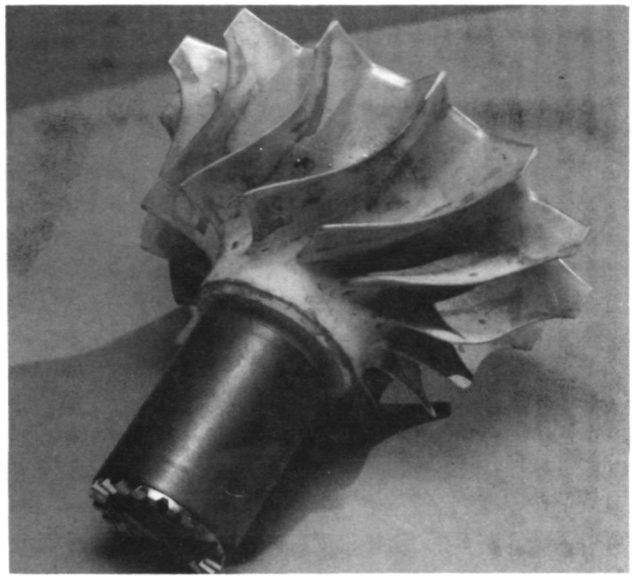

Figure 61. ACC Si_3N_4 Turbine Wheel After Three Cycles.

assembly. A manufacturing sequence/method is being evaluated wherein a dummy shaft will be used and later removed after final grind and prior to final densification of the coating at the vendor (Reference 5).

As stated in Section 4.5.4 herein, two ceramic rotors were hot rig tested. These rotors employed this dual sleeve coupling and operation was satisfactory with no evidence of ratcheting following test. The attachment is considered qualified for operation in this metal engine.

4.6 Rotor Dynamics/Foil Bearing

During this reporting period, a significant amount of rotor dynamic development work, which was necessitated by continuing unstable subsynchronous motion during engine operation was accomplished. This motion is thought to be self-excited because the frequency was related to the first critical mode (rigid body, conical shape) and is related to forced modes at gearbox frequencies. This motion shows very large amplitudes at the turbine (foil bearing) end of the rotor; therefore efforts to solve this problem have been concentrated on the foil bearing. Additionally, the change to a quill shaft type gearbox helped minimize the dynamic motion.

4.6.1 Foil Bearing Dynamic Development

Based on Garrett experience with unstable subsynchronous motion on production air cycle machines, the foil bearing dynamic development has been directed at increasing the bearing stiffness while maintaining high load capacity. Steps in this development included analysis, rig testing and engine testing.

4.6.1.1 Analysis

A recently developed foil journal bearing analysis computer program, developed by Garrett, is being utilized to parametrically study the influence of changing various bearing geometric parameters during development. The analysis provides the simultaneous elastic-hydrodynamic solution for an operating foil bearing. This analysis has been used to screen and optimize the effect of development changes in bearing geometry.

4.6.1.2 Static Bearing Test Rig

The static bearing test rig has been utilized extensively to characterize the load deflection relation of a stationary foil bearing assembly. The static spring rate, while not precisely duplicating the dynamic rate, is a critical bearing parameter in predicting rotor dynamic behavior.

An effort to replicate bearing dynamic spring-rate in the static spring rate test rig was made by utilizing a hydrostatic bearing shaft in the rig. Figure 62 shows the configuration of this shaft. Air pressure sufficient to cause the foils to lift off the shaft was applied and then a deflection versus load curve was plotted, as shown in Figure 63. The results of this testing show a much lower hysteresis loop when the bearing is hydrostatic. Based on these results, efforts are directed toward achieving greater bearing hysteresis, and consequently, damping, while the bearing is hydrodynamic.

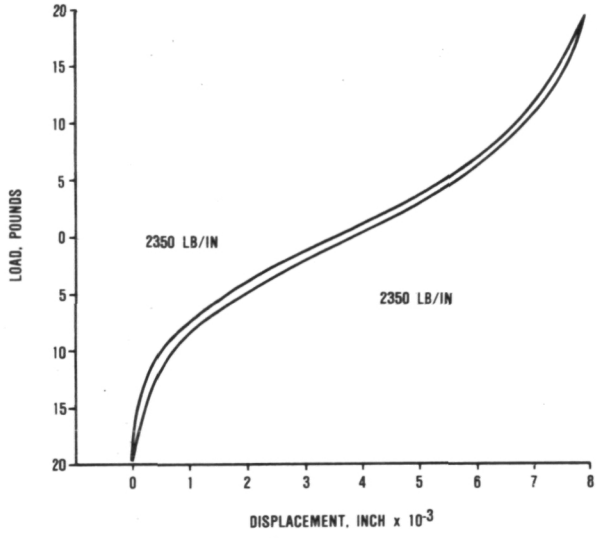

Figure 63. Load Deflection Curve for Standard Engine Bearing Using Hydrostatic Test Journal.

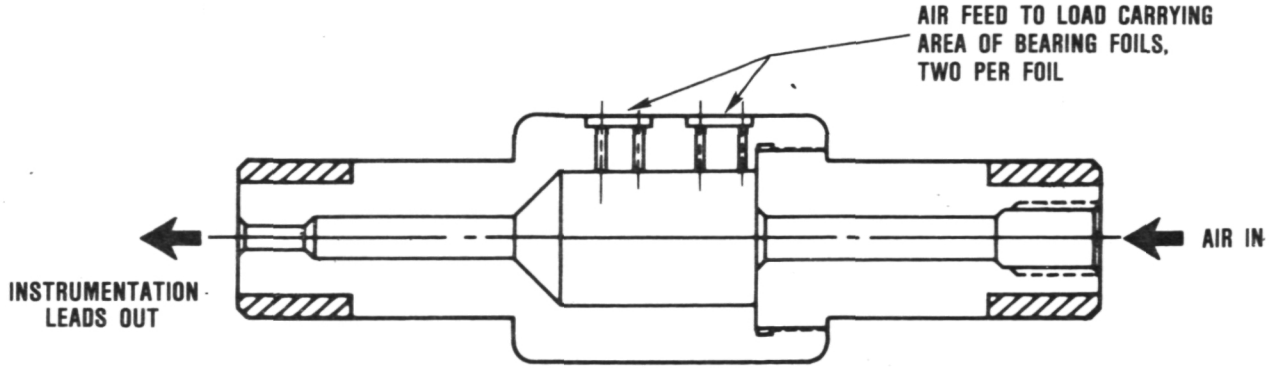

Figure 62. Hydrostatic Journal for Load Deflection Testing of Foil Bearing.

4.6.1.3 Single Bearing Test Rig

Operating bearing characteristics were established on the single bearing test rig. This test rig was specifically designed to provide a dynamically stable test bed for evaluation of bearing performance parameters. The bearing is tested over the design speed range for maximum load capacity, power dissipation, dynamic spring rates, and stability (although the test rig rotor system is inherently stable, unstable bearing designs can be detected). Bearing breakaway torque as well as foil lift-off and touchdown speeds are determined.

Single bearing test rig results for the current baseline engine bearing (teflon coating) are shown in Figure 64 where bearing power dissipation is plotted as a function of load and speed. Figure 65 shows bearing power dissipation plots for a high spring rate bearing being considered for engine use.

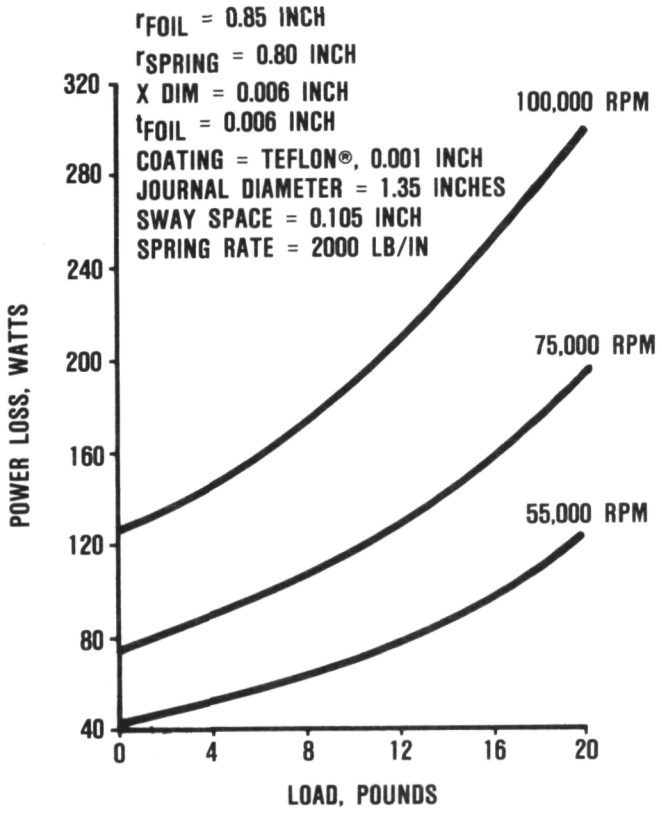

Figure 64. Power Distribution Versus Load at Constant Speed, Engine Baseline Bearing.

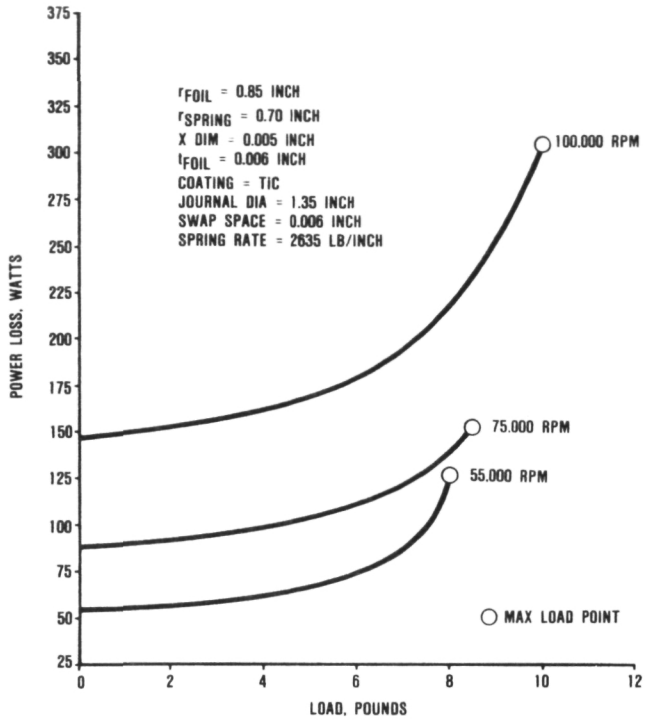

Figure 65. Power Distribution Versus Load at Constant Speed, High Spring Rate Bearing.

4.6.1.4 Bearing Dynamics-Repeatability

Since the successful operation of engine S/N 003 Build 4, evidence accumulated verifies that subtle differences in bearing characteristics can have a significant effect on stable engine operation repeatably.

A thorough procedure was developed to screen bearings dimensionally and on the test rigs to assure acceptable dynamic behavior. At the same time, the manufacturing tolerances have been investigated and a range of bearings tested in an attempt to assure consistent dynamic behavior for all bearings meeting the current blueprints. Materials and processes also will be more closely controlled to enhance repeatability. These procedures have been successful in rig tests, but are not yet proven in engine testing.

4.6.2 Quill-Shaft Gearbox Development

A quill-shaft gearbox was installed on the rotor-dynamics rig for evaluation. This design, shown in Figure 66 utilizes a quill shaft drive from a splined spacer on the compressor shaft to an internally splined ball bearing mounted sun gear. This design eliminated forced subsynchronous motion at the turbine corresponding to ring gear and planet gear frequencies and multiples thereof.

A second quill-shaft gearbox was assembled and tested on the rotor dynamics rig and gave the same results as the first quill-shaft gearbox. The first quill-shaft gearbox then was installed on an engine. Quill-shaft gearbox engine installation resulted in substantial reduction or elimination of subsynchronous motion at the turbine corresponding to ring gear, and planet gear frequencies.

4.7 AGT Controls and Accessories

This reporting period has been spent in completing fabrication and testing of a third electronic control unit and a third fuel control unit and providing support of the engine test program.

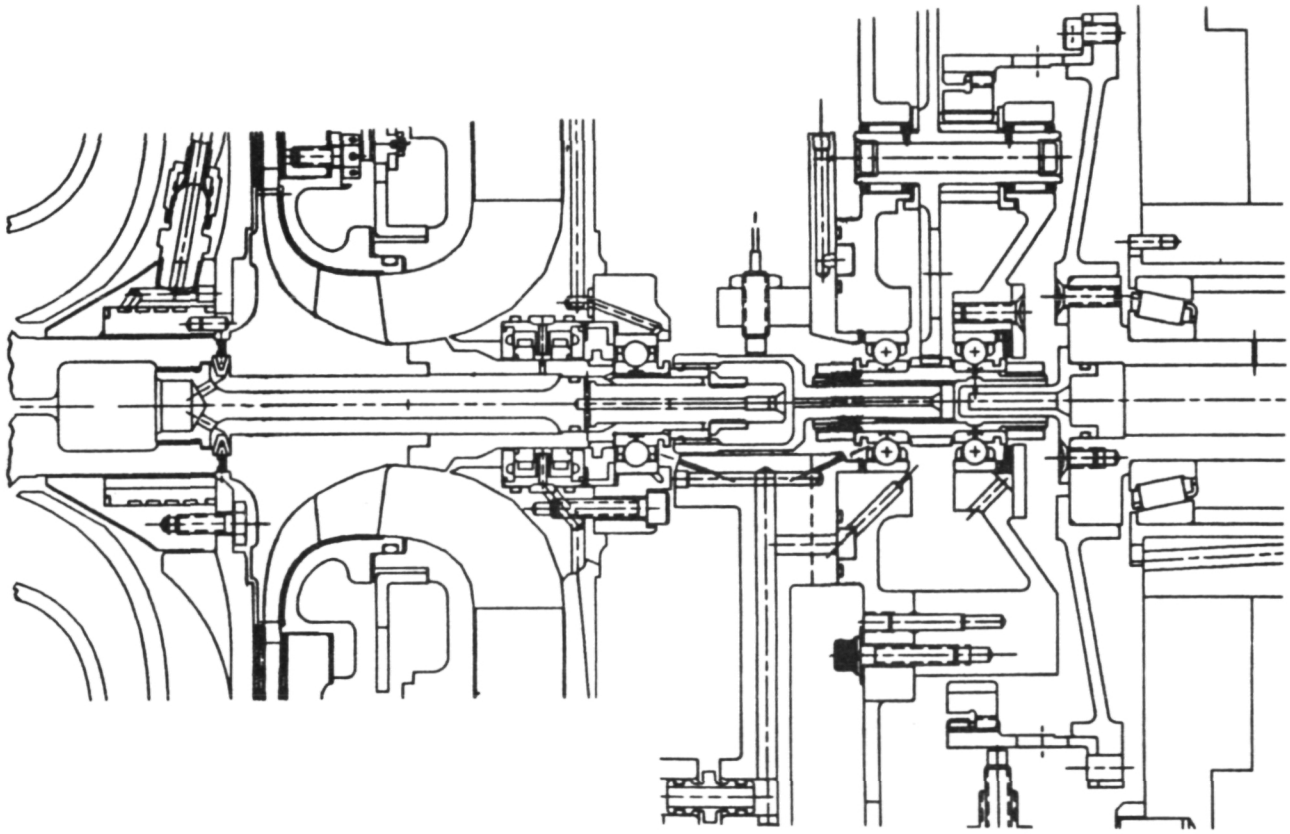

Figure 66. Quill Shaft Gearbox.

APPENDIX A

FORD MOTOR COMPANY
ADVANCED GAS TURBINE (AGT) POWERTRAIN
SYSTEM DEVELOPMENT PROGRAM
SEVENTH AGT SEMI-ANNUAL
TECHNICAL PROGRESS REPORT

1. TASK 2.3 - CERAMIC ROTOR

1.1 Material Development and Characterization

As reported previously in References 5 and 6, sintered reaction bonded silicon nitride (SRBSN) materials developed thus far for rotor application have exhibited a drop in stress rupture strength when tested at 1832°F. Further testing led to the conclusion that this strength loss was due to oxidation occurring at intermediate (1832°F) temperatures. While further work is in progress to develop new generations of materials with inherent oxidation resistance, an improvement in oxidation resistance can be made by preoxidation of the current material, Code RM-2, to provide a dense, glassy oxide surface layer to inhibit further oxidation. This material, Code RM-3, has now been characterized, and the results of this work reported herein.

A group of test samples were machined from larger sintered billets, and subsequently pre-oxidized to form the RM-3 SRBSN material. Fast fracture MOR testing was performed at room temperature, 1832, 2192, and 2552°F. Test results are shown in Table 14, and indicate some drop-off in strength with increasing temperature; this behavior is typical of most Y_2O_3-doped silicon nitride materials, and is consistent with, although slightly lower in strength than data generated previously on RM-2 SRBSN, Reference 4.

Another group of test samples were tested in static (no load) oxidation in an air-atmosphere electric furnace for 300 hours at temperatures of 1292, 1832, 2192, and 2552°F. Weight changes were measured at several time increments during the 300-hour exposure, as depicted in Figure 67. As shown, much of the weight gain occurs during the preoxidation step. Very little additional weight gain takes place at 1292 and 1832°F, a distinct improvement over RM-2 characteristics (Figure 68) and further indicating that the preoxidation treatment prevented oxidation at the intermediate temperatures. A slight weight gain was noted at 2192°F (AGT101 predicted rotor material temperature).

TABLE 14. RM-3 4-POINT MOR FAST FRACTURE STRENGTH

Test Temperature,°F	MOR, ksi	Weibull	n
Room Temperature	98.6	19.0	10
1832	77.6	10.9	5
2192	71.6	12.9	5
2552	70.8	11.3	5

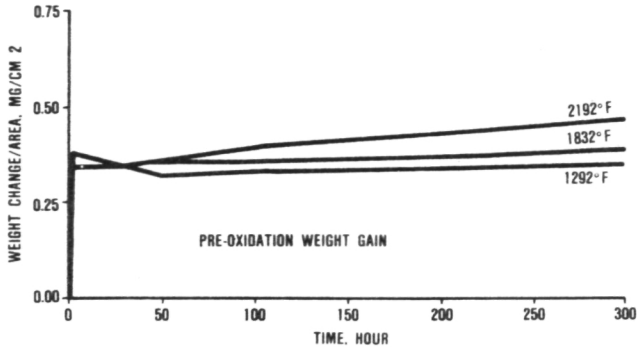

Figure 67. Static Oxidation Weight Change of RM-3 SRBSN Versus Time and Temperature.

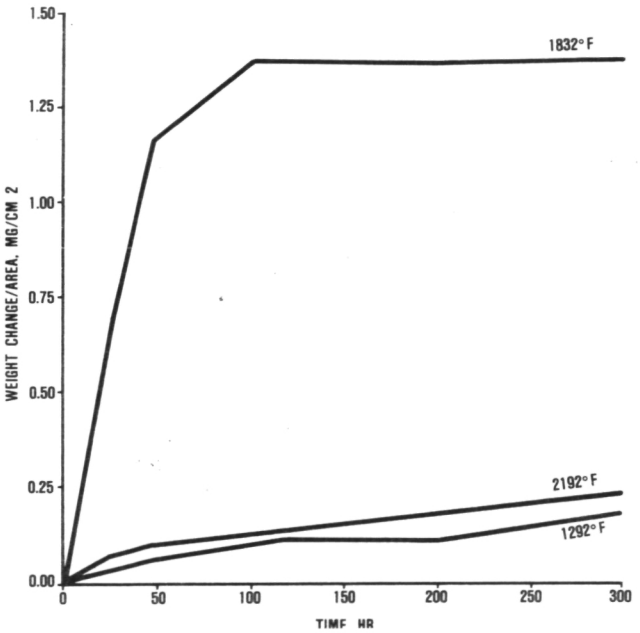

Figure 68. Static Oxidation Weight Change of RM-2 SRBSN Versus Time and Temperature.

After completion of the 300-hour static oxidation testing, all samples were tested in fast fracture MOR at room temperature. Fracture strengths are tabulated in Table 15 and graphically shown in Figure 69. Also included in Figure 69 are comparative data for

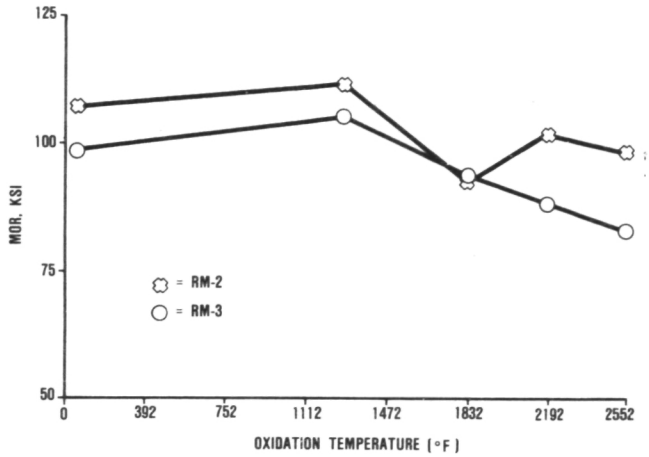

Figure 69. Fast Fracture Room Temperature Strength of RM-2 and RM-3 SRBSN Materials Following 300 Hours Static Oxidation at Various Temperatures.

RM-2 material. The RM-3 material exhibited slightly lower but somewhat more consistent strength than the RM-2 SRBSN.

The most meaningful testing was probably stress rupture. Data on RM-3 stress rupture behavior is shown in Table 16, and includes one step stress rupture test at 1832°F, with increases in applied load taking place at various increments of time. All other test results reported were conducted under constant loading for various times and temperatures. As shown in Table 16, there were no failures at the loads and temperatures tested. The load-carrying ability of RM-3 exceeds the stress rupture requirement of 30 ksi at 2050°F as noted in Reference 4. By contrast, as reported in Reference 5, RM-2 material exhibited a characteristic life of 56 hours at 1292°F and at a load of only 20 ksi.

In summary, this characterization work has shown that RM-3 SRBSN material exhibited substantial improvement in oxidation and stress rupture resistance as compared to the earlier RM-2 material. While further generations of improved SRBSN materials are expected, as a result of continuing material and process research, the RM-3 material has demonstrated adequate high temperature properties to withstand the environment of the

TABLE 15. RM-3 4-POINT MOR STRENGTH AFTER 300 HOUR OXIDATION

Oxidation Temperature °F	MOR, ksi	Weibull	n
1292	105.1	9.21	5
1832	93.8	7.4	5
2192	88.5	12.7	5
2552	83.0	16.4	5

TABLE 16. RM-3 STRESS RUPTURE RESULTS

Temperature °F	Load, ksi	Time, hr	Results
1472	61.8	100	DNF[1]
1832	40	120	DNF
	45	24	DNF
	50	24	DNF
	55	24	DNF
	62	100	DNF
1832	50	240	DNF
1832	50	125	DNF
2192	50	125	DNF
2192	50	105	DNF

[1](DNF) Did Not Fail

AGT101 engine for running times that are anticipated during engine testing in the near future. Materials with improved oxidation resistance are expected to be forthcoming in time for longer duration testing, which may be expected nearer the conclusion of the program.

Test samples were fabricated from a new SRBSN material that may be a candidate to replace RM-3. While similar in composition to RM-3, this material incorporates a small addition of another sintering aid along with the Y_2O_3 normally used. Since only a limited number of samples of this material became available late in the reporting period, it was decided to conduct preliminary stress rupture testing, this being the most meaningful test. A few room temperature fast fracture tests were conducted, establishing that this material has an initial strength of over 100 ksi, although the number of tests performed were not sufficient to establish statistical significance.

Results of the stress rupture tests are given in Table 17. Several samples were

TABLE 17. STRESS RUPTURE RESULTS

Temperature °C	Load, ksi	Time, hr	Results
1472	40	24	DNF[1]
	50	72	DNF
	60	24	DNF
	70	5	F[2] (Internal Void)
1652	40	72	DNF
	50	24	DNF
	60	24	DNF
	70	1	F (Internal Void)
1832	40	24	DNF
	50	24	DNF
	60	72	DNF
	70	24	DNF
	80	24	DNF
2192	40	24	DNF
	50	24	DNF
	60	24	DNF
	70	72	DNF
	80	24	DNF
2050	60	200	DNF

[1](DNF) Did Not Fail

[2](F) Failed

tested in fast fracture room temperature MOR after completion of stress rupture testing, with strength values varying from 115 to 132 ksi. These results are encouraging, and warrant further evaluation of this material.

1.2 Bladed Rotor Fabrication

As noted in Reference 6, basic investigations were undertaken to develop an understanding of slip behavior and the effect of slip properties upon casting behavior. This work has been essentially completed, and resulted in the generation of both physical and chemical models which can be used to predict slip performance.

A method for reducing the chemical activity of the SRBSN that substantially improved slip stability and reproducibility was developed and two bladed rotors were cast. The first of these contained a large open crack in the hub, which was visible immediately after casting This crack was apparently the result of excess shrinkage during casting. Corrections were made in the plaster base, and a second bladed rotor was cast which appeared to be of high quality.

After further processing, this rotor was sintered to a density of 3.24 g/cm^3. Post sintering inspection revealed a few damaged blade tips and a linear indication on one blade root. This rotor is shown in Figure 70 in the as-sintered condition, and is currently being machined preparatory to cold spin testing. This development is considered most promising, and additional bladed rotor casting work is in progress.

As casting quality has improved, it also has become evident that total immersion of the castings in warm (140°F) solvent to remove the wax casting mold was causing considerable damage to the freshly cast rotor, particularly in the thick hub sections. Accordingly, investigations of more gentle wax mold removal methods were undertaken. A new technique was found that appears capable of removing the wax mold without inflicting damage to the delicate rotor casting. Two bladed rotors have been processed, using this latest procedure, which appear to be of high quality; these parts are being nitrided.

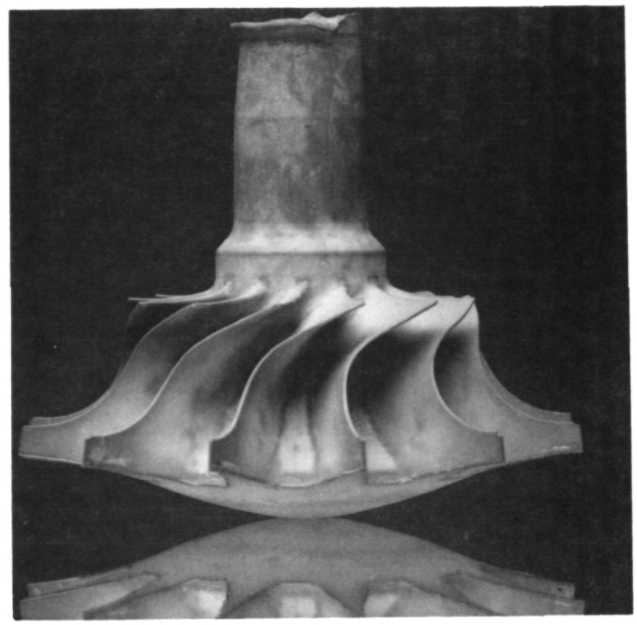

Figure 70. Photograph of Slip Cast Bladed Rotor in the As-Sintered Condition.

2. TASK 2.7 - CERAMIC STATOR

2.1 Molded Stator Processing

As noted in Reference 6, a group of 24 stators were molded late in the reporting period, representing possible deliverable items. These stators were subsequently processed, in small groups, through burnout and nitriding.

The initial group of stators were distorted in the solid shroud following nitriding and were out-of-flat, ranging from 0.010 to 0.081 inch. The cause of this distortion was traced to the ceramic plates used to support the stators during burnout and nitriding, in that these plates were warped; subsequently, the plates were diamond ground to a flat condition. The next group of stators processed through burnout and nitriding using these ground plates exhibited only minor distortion and were well within the allowable clean-up stock limits for finish machining.

Three of this later group of stators were submitted for final machining. One stator was accidentally damaged during machining, while the other two were satisfactorily completed. However, subsequent microscope-aided visual inspection revealed the presence of small, tight cracks in some vane fillet radii, present at both leading and trailing edges, but on the segmented shroud side only. No cracks were observed in these regions on the solid shroud side. These findings were reviewed with Garrett, resulting in a decision to ship these two stators for evaluation in the stator thermal screening rig in order to gain information about the behavior of the monolithic stators in general and the effect of these cracks in particular. An investigation into the cause(s) of these cracks then was initiated.

2.2 Fillet Crack Investigation

The discovery of fillet cracks in the two finish machined stators prompted a re-inspection of all available stators; in total, 34 stators were inspected, including a number of parts molded during earlier parametric studies. Of the group of 24 stators molded under fixed conditions, an average of 7.5 leading edge fillet cracks per stator were detected, with the number of cracks per stator ranging from 1 to 13. Likewise, trailing edge fillet cracks averaged 2.8 per stator, ranging from 0 to 12. Six of these stators had no trailing edge cracks. Of the group molded earlier, a significantly different crack distribution was noted. Two of these were completely free of fillet cracks, and no trailing edge cracks were observed. A consistent pattern of crack distribution, centered around the single point gate, was noted on all cracked stators.

A systematic study then was conducted to establish a relationship between all molding variables involved. Most of these variables were found to produce little effect on the cracks, but gate location, sprue type, injection pressure, and time to open the tool after molding appeared to exert significant influence.

Additional molding experiments have been initiated to evaluate the effects of these four variables upon stator quality.

2.3 Development of SRBSN Stators

Longer range plans have been made to investigate the fabrication of SRBSN integral stators as a potential replacement for RBSN, in order to utilize the improved properties of SRBSN for increased stator reliability.

Molding development for producing SRBSN stators was initiated and directed primarily towards identifying process shrinkage for the integral stators. A batch of material was prepared using a sinterable material formulation which would produce a nitrided density of 2.5 g/cm^3. A batch of 22 stators were molded, varying material temperature from 160 to 200°F, and tool cavity pressure from 2500 to 6500 psi.

All the stators were dimensionally measured after molding and will be monitored for changes when processed through nitriding and sintering. Shrinkage data then will be available, including the effect of any sensitivity to melt temperature and injection pressure.

3. TASK 2.7 - FLOW SEPARATOR HOUSING

While no fabrication or development work was scheduled during this reporting period, negotiations were completed on an order of five more components to be fabricated by Corning in the near future. A purchase order for this work is being processed.

APPENDIX B

AIRESEARCH CASTING COMPANY (ACC) ADVANCED GAS TURBINE (AGT) POWERTRAIN DEVELOPMENT PROGRAM SEVENTH AGT SEMIANNUAL TECHNICAL PROGRESS REPORT

1. SUMMARY

Successful thermal shock testing of bladed rotor, S/N 277, previously spin tested to 115,000 rpm, fully qualifies this rotor for engine use. Rotor fabrication efforts have demonstrated improved visual appearance and increasing yield.

ACC has demonstrated promising sinter/HIP capability. In initial experiments, a bladed rotor was densified to 3.26 g/cm^3 and appeared to remain free of significant defects. Sintering at Ford was continued as the baseline. Delivery of sintered hardware is summarized in Table 18.

Fabrication efforts were initiated on two new RBSN components and re-activated on three which had been on hold. Design changes in the inner and outer diffusers have resulted in changes in the casting approach which, in turn, have greatly assisted fabrication of deliverable hardware. High purity silicon powder from a new source has yielded better castings by improvements in slip properties.

2. ROTOR - MATERIALS AND FABRICATION DEVELOPMENT

Rotor, S/N 277, has been qualified for engine testing by successful completion of 15 percent overspeed testing reported earlier, and thermal shock testing.

Rotor fabrication continued and some key process parameters used in manufacturing S/N 277 were included as a new baseline. For example, the calcining process was discontinued. Heating milled materials in air (calcining) had been performed to provide powder producing more stable slips. The calcining process did result in small internal and surface flaws and some effort had been extended to reduce these flaws by changes in calcining temperature and post calcining milling. Changes in raw material specifications and slip deflocculants, however, demonstrated that calcining was not necessary and all current work is continuing without calcining.

Efforts are continuing to determine optimum deflocculants (dispersants). Four deflocculants are being evaluated, alone and in various combinations. The evaluation criteria for a dispersant include effectiveness in reducing viscosity and improving casting behavior (rate, uniformity, density) of the slip. Optimum deflocculation parameters will change with changing powder conditions.

Using as-received powders (not calcined) and the best dispersion techniques, castings of good visual quality are being produced. However, cracking is still evident in some castings, and can become apparent at any later processing step.

During this reporting period, a significant source of rotor casting cracking was identified and corrected. Wax mold removal procedures, previously considered satisfactory, were affected by increased fabrication time and the recent relocation of facilities. The procedures used appear to have resulted in mold expansion prior to removal. This mechanism had not been apparent earlier and resulted in undue concern for casting and drying limitations. All process steps are now reasonably satisfactory but can be further improved.

Bladed rotor, S/N 344, was successfully

TABLE 18. SUMMARY OF HARDWARE DELIVERY

JANUARY 1 - JUNE 30, 1983

Component	Total Parts Shipped	S/Ns
Bladed Rotor	2	344, 316
Rotor Dynamics	1	315
Test Rotor		
Shaft Attachment	2	352, 345
Test Piece		
Baffle	0*	
Stator	0*	
Shroud	3	288, 194, 215
Inner Diffuser	4	298, 294, 299, 286
Outer Diffuser	3	297, 289, 272
Rings		
Regenerator Seal	0*	
Shroud Seal	8	280-283, 302-305
Wave Washer Spring	0	
Flow Separator Seal	New*	
Outer Diffuser Spacer	New*	

*These components reactivated, or new requests, in the latter part of the reporting period.

densified in the ACC HIP facility to a density of 3.26 g/cm^3 and is the best internally processed rotor to date and was shipped to Garrett for testing. Equipment difficulties delayed the start of processing by the sintering approach and properties, other than density have not yet been measured. Additional equipment modification is necessary to assure reproducibility prior to any work leading to optimization of the sinter/HIP cycle.

Sintering at Ford is continuing. One bladed rotor, S/N 316, and one rotor dynamics test piece, S/N 317, were sintered at Ford and delivered to Garrett for testing. Additional pieces were sintered but not considered suitable for testing due to cracks. These cracks were not obvious prior to sintering but are considered to be most likely the product of earlier processing steps.

A partial densification/presintering process was developed as a result of the continuing ACC low pressure (100 psig or less) sintering experiments. A moderate temperature, low pressure cycle was used to densify rotors from 2.1 g/cm^3 to 2.7 g/cm^3. This process allows shipment by normal commercial routes, closer presintering inspection, and is expected to reduce sintering distortion apparent in some sintering approaches. This process was used to ship one rotor to Ford (yet to be sintered).

In addition to bladed rotors, additional shaft specimens were requested by Garrett. The difficulty in fabrication of the shaft specimen was found to be largely the result of poor mold design and alternate tooling was obtained. Nine new castings are in process in addition to two which have been sinter/HIPped and shipped to Garrett for use.

A new material composition (92-percent Si_3N_4, 6 percent Y_2O_3, and 2 percent Al_2O_3) was introduced to rotor fabrication for evaluation. The original Si_3N_4 composition was developed in the program "Injection Molding of Sinterable Silicon-Base Monoxide Ceramics" under Contract AFML-TR-78-200 completed in 1978. Although the higher Y_2O_3 and Al_2O_3 content (8-percent and 4-percent respectively) was known to have detrimental effects on long term, high temperature properties, this composition was considered suitable for process development and demonstration. The new composition was developed and evaluated in the program "Low Cost, Net-Shape Ceramic Radial Turbine Program" under Contract DAAG46-81-C-0006, and showed improved high temperature strength (65 ksi at 2250°F) compared to the 8-percent Y_2O_3 -4 percent Al_2O_3 composition. Casting results show that the new composition is very suitable for slip casting the AGT101 rotor. Following successful casting results, further efforts were put on hold by Garrett to concentrate efforts on the original process.

3. CERAMIC STRUCTURES

3.1 Combustor Transition

Further activity on this part was put on hold by Garrett due to satisfactory supply on hand for testing.

3.2 Turbine Baffle

Activity on this part was on hold by Garrett throughout most of the reporting period due to the supply on hand and anticipated deliveries. At the close of the reporting period, ACC was requested to reactivate fabrication. Molds were prepared for casting.

3.3 Turbine Stator

Activity on this part was on hold by Garrett throughout the first half of the reporting period due to satisfactory supply on hand for testing. During the second half, the tool was reworked to eliminate excess flash and fifty stators were injected of good visual and x-ray quality. These will be fully processed and shipped.

3.4 Turbine Shroud

Three shrouds, S/Ns 194, 215, and 288 were nitrided and delivered to Garrett for testing. Two more, S/Ns 307 and 308 were in nitriding at the close of the reporting period.

Difficulties in casting the shroud and other static hardware were encountered which were due to the impurity content in the old powder. This was partially overcome by introducing a powder washing process step and introducing a new deflocculant. These were found unsatisfactory due to excess handling in the washing process and the discovery of a harmful residue from the deflocculant found after nitriding. Efforts to produce thicker shrouds (already the thickest part) were especially hampered using the powder on hand.

Excellent casting results had been attained using a high purity powder from an alternate source. One ton of this powder was ordered and one-half was received and is in regular use.

Five additional shrouds were cast and delivered to Garrett for green machining.

3.5 Turbine Inner Diffuser

Four inner diffuser housings (IDH), S/Ns 286, 294, 298 and 299 were nitrided and delivered to Garrett for testing. Two more, S/Ns 309 and 311, were in nitriding at the close of the reporting period. Delivered hardware was of both the original large configuration, resembling a brake drum, and a new, simple disc configuration.

The new configuration IDH is part of an engine "B" design which also modifies the outer diffuser housing (ODH). Both components are designed to be easier to fabricate and be more reliable. Both components can be produced by using tooling built for the original configuration but modifying the manner in which it is used. All current castings are the new configuration.

Six castings, of the new configuration, have been delivered to Garrett for green machining.

3.6 Turbine Outer Diffuser

Three outer diffuser housings (ODH), S/Ns 272, 289 and 297 were nitrided and delivered to Garrett for testing. Two more, S/Ns 296 and 300, were in nitriding at the close of the reporting period.

Use of original tooling for the new configuration resulted in some parts in process which were not satisfactory for use. Additional mold modifications are being made to temporarily correct this, and new tooling is in design.

3.7 Ring Components

Five ring configurations are being machined from three sizes of simple cylinders. Two of these are new requests and all are described below.

Regenerator Seal

This seal is 6.7 inches OD. One cylinder is in machining at ACC.

Shroud Seal

This seal nominally is 9.3 inches OD. Eight rings were nitrided and shipped to Garrett and four more are in nitriding.

Flow Separator Housing Seal

Also nominally 9.3 inches OD, this new component (for RBN-104) is machined from the same cylinder as is made for the shroud seal.

Wave Washer Spring

Also nominally 9.3 inches OD. This ring is machined from the same size cylinder as is made for the shroud seal. Because of the wavy configuration, this component serves as a spring in the axial direction between two flat surfaces. Seven were in nitriding at the close of the reporting period.

Outer Diffuser Housing Spacer

This is a new part required in the redesign of the ODH and is 10.9 inches OD. One cylinder is prenitrided, ready for machining.

Piston Ring

Two rings were nitrided and returned to Koppers Company for final machining. The piston ring seal concept is not being considered, and no additional activity is anticipated.

APPENDIX C

THE CARBORUNDUM COMPANY (UNIQUE WORK) ADVANCED GAS TURBINE (AGT) POWERTRAIN SYSTEM DEVELOPMENT PROGRAM SEVENTH AGT SEMI-ANNUAL TECHNICAL PROGRESS REPORT

1. BACKGROUND

This report summarizes the work carried out by the Carborundum Company during the period January 1, 1983 through June 30, 1983 for the Garrett Turbine Engine Company on the Advanced Gas Turbine Technology Development Program authorized under NASA Contract DEN3-167 and sponsored by the Department of Energy (DOE).

The objective of Carborundum's subcontract from Garrett is to optimize ceramic forming methods utilized in the processing of sintered alpha silicon carbide (SASC) engine components for the hot flow path of the AGT101 engine. In addition, Carborundum has to supply ceramic hardware for test purposes per agreed schedule. Activities during this period were focused on stationary ceramic parts such as the combustor baffle, transition duct, stator segments, turbine shroud, regenerator shield and combustor liner. Injection molding, compression molding, slip casting, extrusion as well as isopressing and green machining were the fabrication processes selected to produce components per the agreed work statement. These different methods are incorporated in the program to utilize the unique advantages of the various processes.

The ceramic fabrication methods chosen have been successfully demonstrated to produce components of variable complexity economically and with high precision. Technical progress has significantly extended near net shape forming capabilities where only minimal grinding is required to obtain a satisfactory finished part.

2. STATIC STRUCTURES

2.1 Stator Segments

The injection molding process has been selected for the fabrication of individual sintered alpha silicon carbide stator segments. During the reporting period, the molding of new stator segments was resumed. An improved injection molding compound made with a different set of plastics was chosen. It produced stator segments virtually free of molding defects or surface imperfections. Differences in shrinkage behavior with the new system necessitated small variations in the plastic content and in the sintering schedule.

The activities on this component are summarized as follows:

- Several batches of stator segments were molded using molding compounds which varied in the plastics content. The mold was originally designed for a composition having 17-percent shrinkage; however, the current improved standard mix exhibits higher shrinkage. Mix modifications proved to be necessary to obtain dimensionally acceptable parts. The plastic amount was highest in the improved standard mix and the subsequent mix variations incrementally incorporated lower amounts of plastics to decrease the overall shrinkage to obtain dimensionally acceptable parts.

Mix	Parts Molded
Improved Standard	20
B-1	125
B-2	150

- o These three sets of stator segments were processed using standard procedures. All parts were then subjected to NDE inspection and a total of 80 parts of each composition B-1 and B-2 passed all tests with the exception of the dimensional analysis. All parts were undersized, with the parts made of compound B-2 being closest to nominal dimensions. In addition, a depression on the trailing edge of the profile was observed.

- o An audit of the various processing steps was undertaken. The following changes were incorporated in the next iteration of moldings:

  - Compounding of one additional mix modification B-3, containing the lowest binder amount of the current system
  - Improved clean-up techniques
  - Modification of sintering schedules
  - Evaluation of sintering fixtures
  - Compounding of mix A, containing the originally used binder system

- o Twenty plastic stator segments were molded to verify the consistency of the mold dimensions and to specifically check the vane shape, vane length, and the profile of the side walls

- o New mixes were compounded and four different lots of stator segments were molded and processed using the changes resulting from the audit:

Mix	Parts Molded
B-1	25
B-2	150
B-3	150
A	200

- o The B compositions yielded highly satisfactory molded parts without apparent flow lines or excessive flash. The stator segments molded with composition A showed slightly unfilled sections and some flow lines

- o All stator segments were processed through binder removal. Subsequent visual inspection rejected all stator segments of composition A and passed the stator segments of the B compositions

- o The sintering fixtures were redesigned incorporating modifications to obtain the proper spacing between the sidewalls and to minimize warpage

- o Various sintering schedules will be investigated using stator segments of the B-2 and B-3 composition. In addition, standard mix will be compounded and processed using standard conditions to determine the exact mold dimensions necessary to obtain acceptable parts

2.2 Turbine Shroud

The turbine shroud has been made by injection molding a thermoplastic alpha silicon carbide mix on a 1000-ton reciprocating screw injection molding machine. During this reporting period, no additional moldings were undertaken because of additional design evaluations and design changes by Garrett. Previously molded and baked parts were processed.

- o A total of six turbine shrouds were completed through grinding and final inspection

- o Four of these showed line indications in inspection and were rejected

- o The remaining two parts passed all NDE inspection steps and were sent to Garrett

- o A modified turbine shroud drawing was obtained and the previously rejected parts

were evaluated according to this new design

- The former design yielded insufficient stock in the vicinity of the reinforced rotor contour and all remaining parts of the old design were discarded

- Design assessment of a new injection molding and/or transfer molding tool has been initiated

2.3 Combustor Baffle

A bimodal slip casting mix has been selected for the fabrication of the combustor baffle in Hexoloy^{TM}SA. The employed method of drain casting yields a reproducible outside configuration but additional green machining is necessary to obtain a defined constant inner contour in connection with a relative large wall thickness (approximately 0.50 inch in the as-cast state).

Compression molding is a second method which will be investigated for this part. This forming process is expected to produce combustor baffles closer to the near net shape and to require no green machining. Preliminary trials gave encouraging results and proper permanent tooling is being designed.

2.3.1 Combustor Baffle (Cast)

- A total of 139 combustor baffles were cast using standard water based bimodal casting slurry. No problems were encountered in obtaining the proper wall thickness

- Some of the baffles cast early during this reporting period exhibited surface flaws after demolding. The main areas of concern were the tab bases and the circumferential seam area

- More frequent mold turnover improved the surface quality and the integrity of the tabs of the as-cast baffles significantly and a slightly larger radius on the tab bases decreased further the rejection-rate due to linear flaws

- Sixty-two baked parts were green machined to a constant wall thickness with sufficient stock on the inside platform and the height

- Problems of edge chipping and cracking during the machining operation were observed on the early parts. Closer inspection of the outside seam area and a modified holding fixture eliminated most of the difficulties

- Thirty-six parts were processed through sintering and were inspected in the as-fired state. Almost all parts exhibited good densities and dimensional control

- The most frequent cause of rejection was a crack on the inside of the nose cone area

- Three combustor baffles that passed all NDE requirements in the as-fired state were shipped with sufficient grinding stock to Garrett

- Seven additional parts that had flaws were also sent to Garrett for evaluation

- Work is proceeding until all delivery requirements have been met

2.3.2 Combustor Baffle (Plastic Forming)

- Work was initiated in June 1983 to develop a plastic forming process to produce combustor baffles to near net shape

- An existing epoxy mold, which was previously used in slip casting, was converted to a simple experimental compression - mold and two compositions using bimodal grain distributions were prepared and molded

- Initial trials showed that the relatively low strength mold material limited the use of high pressures during molding

- Two parts that showed some flow lines and a relatively large parting line in the seam area were processed through binder

removal and will be processed further to provide initial shrinkage data

- A steel compression molding tool is in the design state

2.4 Transition Duct

Isostatic pressing of billets and green machining to net shape was the sequence of processes chosen for the fabrication of transition ducts. CNC lathes and vertical milling machines were used to obtain the specified outside and inside contours and inside platform.

- Work was initiated in February 1983 to deliver four fully machined transition ducts
- Initially isopressed blanks showed defects and the replacement of one component of the isopress tooling was required
- Three green blanks were pressed with the new tooling in place and one of these was green machined using a modified green machining program for the CNC lathe which incorporated additional stock in the platform area
- The green machined transition duct passed inspection, was sintered, and subsequently submitted for as-fired NDE
- Isopressing of four new blanks was initiated and green machining of the remaining two blanks scheduled for July 1983

2.5 Combustor Liner, Regenerator Shield

The newly developed plastic extrusion process was chosen for the fabrication of sintered alpha silicon carbide combustor liners and regenerator shields. These parts previously have been made by isopressing and green machining. The new process was chosen because it has the potential for high volume inexpensive fabrication.

- Work 1983 on these components was initiated in May and preliminary tasks carried out
- Extrusion mix has been compounded and extrusion dies and sintering fixtures received
- The extrusion run has been scheduled for July 1983

3. SUMMARY

- Stator Segments: Approximately 300 stator segments using three mix modifications were molded early during this reporting period. All parts were subjected to standard processing procedures. None of these stator segment sets yielded dimensionally acceptable parts. New stator segments were molded and are processed using modified clean-up techniques, sintering fixtures, and sintering schedules
- Turbine Shroud: All work on the previously molded turbine shrouds has been completed. Apart from the design assessment task, no additional activities have been scheduled
- Combustor Baffle (Cast): Early during this reporting period, difficulties were observed on the as-cast hardware due to mold imperfections and in green machining due to fixturing problems. Corrective actions resulted in significant improvements with respect to surface finish, tab integrity, and dimensional control
- Combustor Baffle (Plastic Forming): To date, only preliminary work has been initiated on this new concept of compression molding baffles with as-molded inside and outside contours which require no green machining and only minimal grinding
- Transition Duct: Initial isopressing problems have been resolved and work is progressing according to the revised schedule
- Combustor Liner, Regenerator Shield: The work carried out under this task is slightly behind schedule, but no major problems are expected in the extrusion of these various diameter tubes of relatively short length

APPENDIX D

LIST OF SYMBOLS, ABBREVIATIONS AND ACRONYMS

Acronyms	Definition
ACC	AiResearch Casting Company
AGT	advanced gas turbine
AGT101	the AGT model being developed by Garrett/Ford
Al_2O_3	aluminum oxide
AS	aluminum silicate
BN	Borazon
^oC	degrees Celsius
CBO	The Carborundum Company
C_L	clearance probes
CFDC	Combined Federal Driving Cycle
CNC	computer numerical control
CO	carbon monoxide
CO_2	carbon dioxide
DAW	dual alloy wheel
dB	decibels
DFC	diffusion flame combustor
DOE	U.S. Department of Energy
DS	directionally solidifed
ECU	electronic control unit
EDX	energy dispersive X-ray
EPA	Environmental Protection Agency
^oF	degrees Fahrenheit

LIST OF SYMBOLS, ABBREVIATIONS AND ACRONYMS (Contd)

Acronyms	Definition
Ford 707	an industrial gas turbine engine by Ford
FY	fiscal year
GE	General Electric Company
HC	hydrocarbon
HCl	hydrogen chloride
Hexoloy^{TM} KX01	Carborundum material, SiC
Hexoloy^{TM} KX02	Carborundum material, SiC
Hexoloy^{TM} SA	Carborundum material, SiC
Hf	halfnium
HIP	hot isostatic pressing
HP	high pressure regenerator inlet (cold side)
HPSN	hot pressed silicon nitride
hp	horsepower
HTC	Heat transfer coefficient
Hz	Hertz (frequency)
ID	inner diameter
IDH	inner diffuser housing
IGV	inlet guide vane (compressor)
IR&D	internal research and development
I-112	regenerator seal coating material
JP-4	jet propulsion fuel Number 4
ksi	thousand pounds per square inch
lb/min	pounds per minute

LIST OF SYMBOLS, ABBREVIATIONS AND ACRONYMS (Contd)

Acronyms	Definition
LAS	Lithiium aluminum silicate
LBO	lean blowout
LCF	low cycle fatigue
LDV	laser Doppler velocimeter
LHV	lower heating value
LP	low pressure regenerator inlet (hot side)
"m"	Weibull modulus
MAS	magnesium aluminum silicate
MEK	methyl ethyl ketone
MENTOR II	Ford regenerator computer program
METCO 443	flame spray coating
METCO 447	flame spray coating
MgO	magnesium oxide
Mod I	first development engine
Mod II	second generation ceramic engine
MOR	modulus of rupture
N	rotational speed
N_{ps}	population, number of samples
NASA	National Aeronautics and Space Administration
NGK	NGK-Locke, Inc.
NiCr	nickel chrome alloy
NO_x	oxides of nitrogen
OD	outer diameter

LIST OF SYMBOLS, ABBREVIATIONS AND ACRONYMS (Contd)

Acronyms	Definition
ODH	outer diffuser housing
PM	powder metal
P/N	part number
PPH	pounds per hour
PR_C	compressor pressure ratio
P_S	static pressure
PR_T	turbine pressure ratio
psia	pounds pressure per square inch, absolute
psid	pounds pressure per square inch, differential
psig	pounds pressure per square inch, gauge
P_T	total pressure
PWM	pulse width modulated
RBN 104	ACC RBSN material
RBN 124	ACC RBSN material
RBSiC	reaction bonded silicon carbide
RBSN	reaction bonded silicon nitride
RM-1	Ford rotor material, first generation
RM-2	Ford rotor material, second generation
RM-3	Ford rotor material, third generationRMS
RPD	reference powertrain design
rpm	revolutions per minute
RSSiC	reaction sintered silicon carbide
SASC	Sintered alpha silicon carbide

LIST OF SYMBOLS, ABBREVIATIONS AND ACRONYMS (Contd)

Acronyms	Definition
SEM	scanning electron microscopy
SiC	silicon carbide
Si_3N_4	silicon nitride
SLE	Straight line element
SMD	sauter mean diameter
S/N	serial number
SNN 522	ACC sintered silicon nitride
SN-50	NGK silicon nitride material
SR	stress rupture
SRBSN	sintered RBSN
SSN	sintered silicon nitride
SWH	seal working height
TC	thermocouple
TD	theoretical density
TIR	total indicator reading
TIT	turbine inlet temperature
TRW	Thompson Ramo Woldridge, Inc.
T_T	total temperature
T-T	total-to-total
VIGV	variable inlet guide vane
VSTC	variable stator torque converter
W_t	speed
W	tungsten

LIST OF SYMBOLS, ABBREVIATIONS AND ACRONYMS (Contd)

Acronyms	Definition
W-K	Wayne-Kerr
yo-yo	Astroloy heat treat cycle
Y_2O_3	yttrium oxide
α-SiC	Carborundum material, Hexoloy™
β	beta
ΔT/T	temperature/temperature standard
μ	micro strain
ΔP/P	pressure/pressure standard
A	characteristic strength

REFERENCES

1) Garrett Turbine Engine Company, "Advanced Gas Turbine (AGT) Powertrain System Development for Automotive Applications", Semiannual Progress Report Number 1 (October 1979 through June 1980), Report No. NASA CR- 165175, November 1980, Contract No. DEN3-167.

2) Garrett Turbine Engine Company, "Advanced Gas Turbine (AGT) Powertrain System Development for Automotive Applications", Semiannual Progress Report Number 2. (July 1980 through December 1980), Report No. NASA CR-165329, June 1981, Contract No. DEN3-167.

3) Garrett Turbine Engine Company, "Advanced Gas Turbine (AGT) Powertrain System Development for Automotive Applications", Semiannual Progress Report Number 3 (January 1981 through June 1981), Report No. NASA CR- 167901, December 1981, Contract No. DEN3-167.

4) Garrett Turbine Engine Company, "Advanced Gas Turbine (AGT) Powertrain System Development for Automotive Applications", Semiannual Progress Report Number 4. (July 1981 through December (1981), Report No. NASA CR-167983, June 1982, Contract No. DEN3-167.

5) Garrett Turbine Engine Company, "Advanced Gas Turbine (AGT) Powertrain System Development for Automotive Applications," Semiannual Progress Report Number 5. (January 1982 through June 1982), Report No. NASA CR-168104, December 1982, Contract No. DEN3-167.

6) Garrett Turbine Engine Company, "Advanced Gas Turbine (AGT) Powertrain System Development for Automotive Applications," Semiannual Progress Report Number 6. (July 1982 through December 1982), Report No. NASA CR-168246 June 1983, Contract No. DEN3-167.

7) Bruce, T.W., H.C. Mongia, and R.S. Reynolds, "Combustor Design Criteria Validation, Volume I - Element Tests and Model Validation," USARTL-TR-78-55A (AD-A067657) 1979.

8) Houtman, D.J., F.L. Dryer, K.P. Schug, and I. Glassman, "A Multi-Step Overall Kinetic Mechanism for the Oxidation of Hydrocarbons," Comb. Sci. Tech., pp. 25, 219-235 (1981).

9) Anderson, D.N., "Ultra-Lean Combustion at High Inlet Temperatures", Report No. NASA TM-81640, Prepared for Twenty-Sixth Annual International Gas Turbine Conference (March 8-12, 1981), Interagency Agreement EC-77- A-31-1011.

1 Report No	2. Government Accession No.	3 Recipient's Catalog No
NASA CR-174694		

4 Title and Subtitle	5 Report Date
Advanced Gas Turbine (AGT) Powertrain System Development for Automotive Applications Fifth Semiannual Progress Report (January 1983 - June 1983)	December 1983
	6 Performing Organization Code
7 Author(s)	8. Performing Organization Report No
Engineering Staff of Garrett Turbine Engine Company, A Division of the Garrett Corporation	31-3725(7)
	10. Work Unit No
9 Performing Organization Name and Address	11 Contract or Grant No
Garrett Turbine Engine Company Division of Garrett Corporation P. O. Box 5217 Phoenix, Arizona 85010	DEN3-167
	13 Type of Report and Period Covered
12 Sponsoring Agency Name and Address	Interim, January June 1983
Department of Energy Division of Transportation Energy Conservation Washington, D.C. 20545	14 Sponsoring Agency Code
	DOE/NASA/0167-7

15 Supplementary Notes

Interim Progress Report under Interagency Agreement
Project Manager R. Palmer, Transportation Propulsion Division, NASA-Lewis Research Center, Cleveland, Ohio 44135

16 Abstract

This report is the seventh in a series of Semiannual Technical Summary reports for the Advanced Gas Turbine (AGT) Powertrain System Development Project, authorized under NASA Contract DEN3-167, and sponsored by the Department of Energy (DOE). This report has been prepared by Garrett Turbine Engine Company, A Division of the Garrett Corporation, and includes information provided by Ford Motor Company, the Carborundum Company, and AiResearch Casting Company. The project is administered by Mr. Roger Palmer, Project Manager, NASA-Lewis Research Center, Cleveland, Ohio. This report presents plans and progress for the period January through June 1983.

17 Key Words (Suggested by Author(s))	18 Distribution Statement
Advanced Gas Turbine Single Shaft Engine Ceramic Turbine Turbine Transmission	Unclassified - Unlimited Star Category 85 DOE Category UC-96

19 Security Classif (of this report)	20. Security Classif. (of this page)	21 No. of Pages	22 Price*
Unclassified	Unclassified	68	

* For sale by the National Technical Information Service, Springfield, Virginia 22161